https://doi.org/10.5194/egusphere-2026-3186
Preprint. Discussion started: 18 June 2026

From *Phaeocystis* to *Chaetoceros*: silicic acid as the primary driver of diatom bloom magnitude in an Arctic mesocosm experiment

Antonia U. Thielecke[1], Clara J.M. Hoppe[1], Jeffrey W. Krause[2,3], Sarah Lena Eggers[1], Uwe John[1], Dave Clarke[4], Martin Whitehouse[5], Heejin Jeon[5], Nicolè Caputo[4,6], Francesca Cucchi[4,6], Amanda Curtin[4], Mar Fernández-Méndez[7]

[1]Alfred Wegener Institute Helmholtz Center for Polar and Marine Research, Bremerhaven, Germany
[2]Dauphin Island Sea Lab, Dauphin Island, AL, USA
[3]University of South Alabama, Mobile, AL, USA
[4]Marine Environment and Food Safety Services, Marine Institute, Rinville, Oranmore, Galway, Ireland.
[5]Swedish Museum of Natural History, Stockholm, Sweden
[6]Marine and Freshwater Research Centre, Atlantic Technological University, Galway, Ireland
[7]University of Bremen, Bremen, Germany

Correspondence to: Antonia U. Thielecke (Antonia.thielecke@awi.de)

Abstract. The phytoplankton spring bloom constitutes the majority of annual Arctic primary production. In the Eurasian Arctic it is usually composed of various diatoms and the haptophyte *Phaeocystis*; recently, *Phaeocystis*-dominated blooms seem to be expanding. Low silicic acid (Si) availability has been hypothesised to promote *Phaeocystis* blooms, though the key drivers of *Phaeocystis* and diatom competition are not yet well understood. To investigate how Si availability controls bloom succession and biogeochemical fluxes we conducted a 3-week mesocosm experiment in Kongsfjorden, Svalbard in May 2024 on the spring phytoplankton community. The initial phytoplankton community was composed predominantly of *Phaeocystis* and the diatom *Chaetoceros*. Eight 450-L mesocosms received an Si gradient (0–40 µM) with nitrogen and phosphorus additions every 48 hours and we tracked nutrient uptake rates, community composition, elemental cycling and export. The nutrient additions stimulated phytoplankton growth across all Si levels. Phase I (Days 0–14) was dominated by a *Phaeocystis* bloom, terminating synchronously due to nitrogen and phosphorus depletion despite variable Si availability. In phase II (Days 16–22) *Chaetoceros* emerged as the dominant species with clear Si gradient effects: *Chaetoceros spp.* sustained exponential growth (μ = 0.40 d^{-1}) and achieved higher abundances in >3 µM Si treatments, while collapsing in Si-depleted mesocosms. Overall, particulate organic carbon export fluxes were low, but were strongly correlated with biogenic silica export fluxes, and increased exponentially in phase II of the experiment reflecting increasingly diatom-dominated sinking material. Our results demonstrate that Si availability does not govern initial *Phaeocystis*–diatom competition, but is the primary determinant of diatom bloom magnitude. The nutrient storage capacity of *Chaetoceros* confers resilience under transient depletion, while micrograzing and viral infection further mediate community successions. This study underscores the importance of integrating cell-specific and ecosystem-level measurements over extended timescales when predicting climate-driven shifts in Arctic primary production and carbon export.

https://doi.org/10.5194/egusphere-2026-3186
Preprint. Discussion started: 18 June 2026

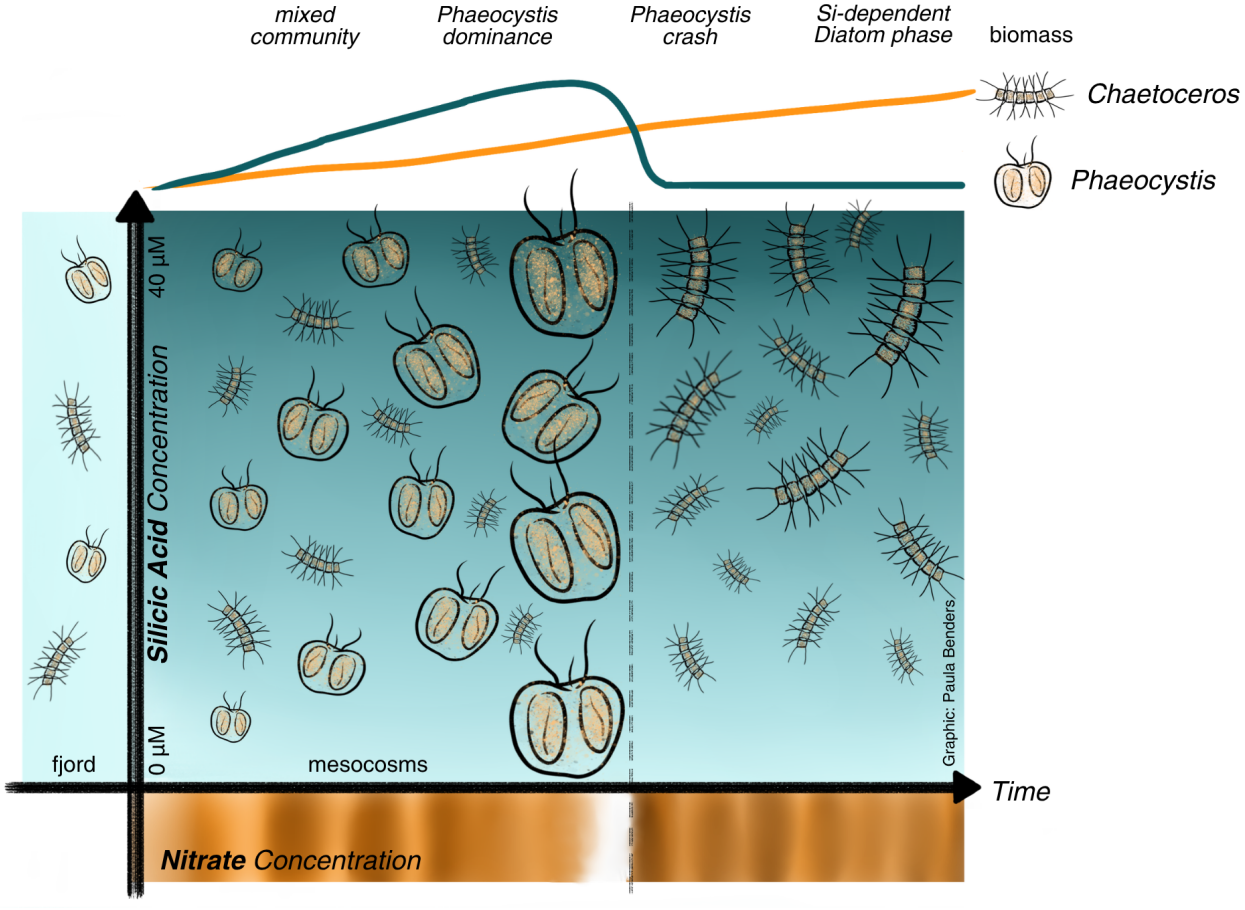

1 Introduction

The Arctic spring bloom that occurs following the polar night is the main annual pulse of primary productivity in the Arctic and underpins food webs and carbon cycling. Despite only lasting weeks, the spring bloom constitutes a major fraction of annual primary productivity (Mikkelsen et al., 2008; Renaut et al., 2018). In recent decades, the Arctic Ocean has been rapidly changing in response to ongoing climate change. Around Svalbard as well as the wider Barents Sea and Atlantic inflow region changing sea ice dynamics and Atlantification have been identified as key driving forces of change (Årthun et al., 2012; Chatterjee et al., 2024; Polyakov et al., 2017; Wang et al., 2020). Atlantification describes the increasing penetration of warm, saline Atlantic Water into the Arctic Ocean and the associated weakening of the halocline, which historically insulated surface waters and sea ice from subsurface heat (Polyakov et al., 2017). This process contributes to sea ice retreat, increased primary productivity in newly open waters, and a borealization of Arctic ecosystems i.e. a shift towards Atlantic-affiliated species assemblages (Husson et al., 2024). Warmer temperature and melting sea ice affect light and nutrient conditions across the

https://doi.org/10.5194/egusphere-2026-3186
Preprint. Discussion started: 18 June 2026

Arctic and as a result changing timing, magnitude and community composition of the spring bloom (Ahme et al., 2023; Bhatt et al., 2014).

The spring bloom in the wider Svalbard area is largely composed of diatoms and haptophytes (i.e. *Phaeocystis pouchetii*) (Assmy et al., 2023; Hoppe et al., 2024; Nöthig et al., 2015). The dominant diatoms during this period are classic spring-bloom r-strategists (Behrenfeld et al., 2021; Glibert, 2016). They are fast-growing, and often dominate early blooms across the European Arctic, including Svalbard, Fram Strait and Barents Sea (Ardyna et al., 2020; Krause et al., 2018). In addition to nitrate and phosphate, they have an obligate requirement for silicic acid (hereafter referred to as Si) to build their frustules. In Fram strait a majority of organic carbon export is linked to sinking diatoms as these frustules act as ballast of single cells, aggregates or fecal pellets promoting efficient carbon export to the benthos or deep ocean (Lalande et al., 2011; Ramondenc et al., 2025). Historically, the early phases of the spring bloom along the marginal ice zone have been diatom-dominated succeeded by a bloom of *Phaeocystis pouchetii* (hereafter referred to as *Phaeocystis*, *Phaeocystis* spp. is used when referring to multiple species; (Wassmann et al., 1999; Weisse et al., 1986)). However, *Phaeocystis* has been increasingly reported to start and dominate the spring bloom (Assmy et al., 2023; Dąbrowska et al., 2025; Nöthig et al., 2015) and has been observed to form extensive under-ice blooms before the ice break up (Ardyna et al., 2020; Assmy et al., 2017). *Phaeocystis* is a rapidly growing, bloom forming haptophyte species occurring in both single cell as well as a colonial stage reaching up to 2mm in diameter. *Phaeocystis* is grazed upon by a wide range of organisms (Admiraal and Venekamp, 1986; Kuhlisch et al., 2020; Nejstgaard et al., 2007; Weisse et al., 1994), yet colony formation constitutes an effective defence against size-selective feeding: small copepods are largely unable to ingest colonies, whereas large copepods such as *Calanus* spp. can feed on colonial *Phaeocystis* (Nejstgaard et al., 2007). Microzooplankton actively graze on solitary cells but are generally unable to ingest intact colonies, and high microzooplankton grazing pressure on solitary cells may itself promote the colonial life stage (Stelfox-Widdicombe et al., 2004). Despite constituting a substantial fraction of spring bloom biomass, evidence for efficient trophic transfer of *Phaeocystis* carbon to higher levels remains conflicting (Nejstgaard et al., 2007; Weisse et al., 1994), with reported grazing rates varying widely across studies. Due to their mucilaginous colony matrix *Phaeocystis* demonstrate slow sinking speed and the dissolution of the colonial matric releases dissolved organic carbon, which fuels bacterial production within the euphotic zone and contributes to the microbial loop (Wassmann, 1994; Wassmann et al., 1990). However, intact colonies and TEP-associated aggregates can also be exported below the euphotic zone, contributing to biological pump dynamics (Reigstad and Wassmann, 2007; Wassmann, 1994). Hence, the composition of the spring bloom and the community succession affects the efficiency of trophic transfer and carbon export (Assmy et al., 2023).

Although the relationship between diatoms and *Phaeocystis* spp. has been extensively studied in the Arctic (Assmy et al., 2023; Degerlund and Eilertsen, 2010; Hegseth et al., 2019; Hegseth and Tverberg, 2013; Hodal et al., 2012; Hoppe et al., 2024) and across the global ocean (Schoemann et al., 2005; Verity et al., 2007) and references therein) the precise mechanisms deciding on the key bloom forming species in a given year is still unclear. *Phaeocystis* blooms have been tied to low Si availability, favouring *Phaeocystis* over diatoms when Si concentrations are depleted <1 µM or in areas with high NO_3:$Si(OH)_4$ ratios (Ardyna et al., 2020; Assmy et al., 2017). There is existing evidence for Si limitation of diatom productivity in the

https://doi.org/10.5194/egusphere-2026-3186
Preprint. Discussion started: 18 June 2026

Eurasian Arctic (Fernández-Méndez et al., 2015), including Si limitation terminating diatom-dominated spring blooms (Krause et al., 2019) potentially contributing to the success of *Phaeocystis*. In Svalbard fjords and Fram strait *Phaeocystis* blooms are often associated with warmer Atlantic inflow waters and increasing presence has been linked to progressing Atlantification and warm temperature anomalies (Assmy et al., 2023; Bracher et al., 2026; Hoppe et al., 2024).

In order to shed light on the role of Si as a regulator of the spring bloom community composition, we conducted a mesocosm experiment incubating the spring bloom community of Kongsfjord, Svalbard, for 3 weeks under a gradient of Si concentrations. Mesocosm experiments combine high ecosystem complexity under natural ecosystem conditions with the opportunity to manipulate and monitor distinct water bodies over extended periods of time (Riebesell et al., 2013). The experiment was conducted shortly before the peak of the spring bloom with comparable presence of *Phaeocystis* and the diatom *Chaetoceros spp.* (hereafter referred to as *Chaetoceros;* although *Chaetoceros gelidus* was the dominant species, multiple species were present and *Chaetoceros* was assessed at genus level throughout the manuscript) as main contributors to phytoplankton biomass. The objective of this study was to understand if Si availability is a key reason for seasonal *Phaeocystis* vs diatoms dominance and to test if there is a threshold concentration that determines the respective dominance. Furthermore, we wanted to test how the ratio between diatoms and *Phaeocystis* affects primary productivity and export production.

2 Materials & Methods

2.1 Study Area

The mesocosm experiment took place in Kongsfjorden, a dynamic Arctic glacial fjord located on the western coast of Spitsbergen in the Svalbard archipelago (79°N), influenced by the convergence of Atlantic and Arctic waters (Fig. 1). The hydrography of Kongsfjorden is primarily shaped by the interplay between warm Atlantic Water (AW) from the West Spitsbergen Current (WSC) and cold Polar Water (PW) from the Arctic Ocean (Hop et al., 2006). The WSC transports AW northward along the western Svalbard shelf, introducing heat and salinity into the fjord, while PW contributes colder, fresher water. Seasonal dynamics, such as summer intrusions of AW, significantly alter the fjord's water column, switching it from Arctic-dominant to Atlantic-dominant conditions (Cottier et al., 2005). Due to the location of the permanent Ny-Ålesund research station, the spring bloom dynamics in Kongsfjorden have been regularly monitored (Hegseth et al., 2019; Hodal et al., 2012). In the last decade several long-term monitoring programs have been established to capture the seasonal variability of the entire suite of hydrography, chemistry, phytoplankton and zooplankton at the base of the foodweb (Assmy et al., 2023; Hegseth and Tverberg, 2013; Hoppe et al., 2024) . Hence, Kongsfjorden is an optimal location to study the interplay of diatoms and *Phaeocystis* and place the conclusion of our mesocosm study in the context of a wider ecosystem understanding.

https://doi.org/10.5194/egusphere-2026-3186
Preprint. Discussion started: 18 June 2026

Figure 1: Overview of experimental settings. (a) Location of Svalbard in the Arctic, (b) Kongsfjorden on the west coast of Svalbard and (c) mooring site of the mesocosms in Ny-Ålesund harbour. Map (a) modified from Humpert (2016), map (b) and (c) modified from Norwegian Polar Institute (2026).

2.2 Mesocosm design

The mesocosms were cone-shaped (around 2 m length and 1 m diameter in the widest part) plastic bags and have a volume of ~450L (Fig. 2b). They were manufactured from clear polyurethane (1mm thickness) with a gas-tight lid (ø 20cm) at the top for sampling and nutrient additions and a sediment trap at the bottom to collect sinking materials (Fenotec, Beelitz, Germany). The sediment trap consisted of a 50cm tube for a total volume of ~1L, closed at the bottom with a rubber plug and connected to the mesocosm with a ball valve, which allowed to close the mesocosm and detach the tube for sampling and emptying of the sediment trap. An encasing mesh was used to facilitate handling and moor the mesocosms in place. A bike valve in the lid was used to inflate the headspace after sampling to ensure mesocosm stability and buoyancy, while a 0.5kg weight attached to

https://doi.org/10.5194/egusphere-2026-3186
Preprint. Discussion started: 18 June 2026

the sediment trap ensured an upright position in the water column. Within the harbour the mesocosms were moored in between swimming piers, centered in the middle of a boat box to reduce shading. A pulley system allowed to move the mesocosms closer to the pier for sampling.

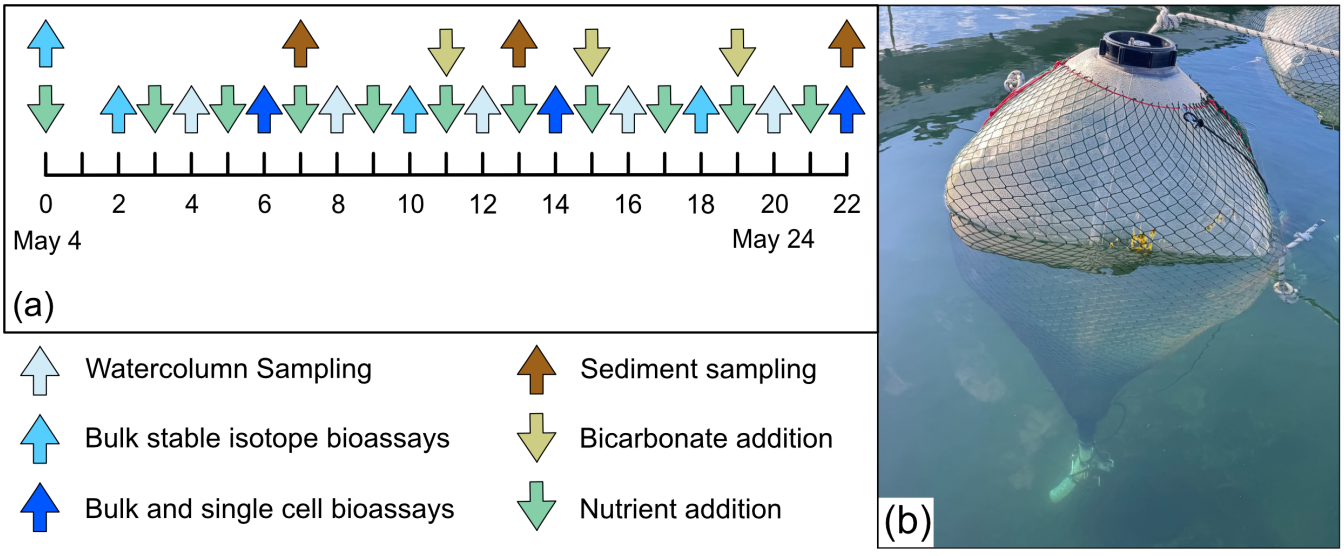

Figure 2: Schematic of sampling schedule (a) and image of a mesocosm (b).

2.3 Mesocosm filling, maintenance and nutrient addition

Eight mesocosms were filled on May 3, 2024 outside of Ny-Ålesund harbour close to the regular monitoring site Kb3 around 78° 55.9' N and 011°56.8' E using AWIPEVs (French-German research base) research vessel Jean Floc'h. The mesocosms were filled with surface water by submerging them from the side of the boat. A 200µm mesh covering the inlet was used to exclude larger grazers and *Phaeocystis* colonies. A maximum of three mesocosms could be filled in one boat trip. All mesocosms were filled within 8 hours and mesocosms from the different sampling trips were randomized in the mesocosm setup and across the nutrient gradient. Volume differences were estimated based on the level of submergence when fully inflated, and up to 60L were exchanged between mesocosms to ensure equal volumes (within 20-30L). Initial sampling confirmed that the phytoplankton community composition was similar across all mesocosms. However, two mesocosms (5 and 40 µM Si) had a reduced overall biomass compared to the other mesocosms corresponding to 66% of the average Chl concentration.

Photosynthetically active radiation (PAR) within the mesocosms at around 50cm depth was measured once on day 6 using a submergeable light sensor (Li-1000, Li-cor, Lincoln, USA). Continuous light and temperature monitoring was obtained from temperature and light pendant loggers (HOBO, Li-cor, Lincoln, USA) tied to the mesocosm lids and weighed down to be oriented vertically in the water column inside the mesocosms. If necessary, ice and snow were removed from the top of the mesocosms during the daily sampling. Once per week, after the emptying of the sediment trap, the mesocosms were cleaned

https://doi.org/10.5194/egusphere-2026-3186
Preprint. Discussion started: 18 June 2026

from the outside to remove the growth on the mesh encasement. Growth on the polyurethane wall was not observed either from the outside or inside of the mesocosms and was therefore deemed negligible.

A Si gradient ranging from 0 to 40 µM (0, 1, 2, 3, 6, 10, 20, 40 µM) was established across the 8 mesocosms. Together with Si, every mesocosm received nitrate and phosphate aiming for 10 µM of nitrate and 0.6 µM of phosphate during nutrient addition every two days (Fig. 2a). Initial nutrient concentrations after filling of the mesocosms were depleted due to the ongoing bloom to below the detection limit for nitrate and around 0.4 µM for dSi. Nutrient additions started on the evening of May 4, (hereafter referred to as day 0 of the experiment) after the initial sampling of the experiment. For the first nutrient addition, mesocosm volumes were estimated to be around 450 L. Nutrient additions were prepared using sodium nitrate, disodium hydrogen phosphate and sodium meta silicate stock solutions for preparation of F/2 medium (Guillard and Ryther, 1962). The nutrients were added to the filtrate obtained from each mesocosms when sampling for Chl, pigments and particulate organic matter (TPC, POC/PON, POP, BSi) which was then added back to the mesocosms to pre-dilute the stock solutions and to reduce the mesocosm volume lost through sampling activities throughout the experiment. This resulted in minor dilutions of around 2% of the total mesocosm volume on a given day, thus dilution was not considered in later accumulation rate calculations. Nutrient samples were always taken immediately before and after the nutrient addition following thorough mixing to evaluate the success of the intended nutrient addition. Based on Si concentrations, the desired nutrient additions were achieved from day 3 onwards following corrections regarding the estimated mesocosm volumes. There were no significant differences between the mesocosms for nitrate or phosphate concentrations. The realised average concentrations were 9.12±1.86 µM of nitrate (mean±SD) and 0.63±0.27 µM of phosphate. Measured Si concentrations on average were in good agreement with the intended Si concentrations (Fig. A1).

Due to the closed design of the mesocosms preventing air-sea gas exchange except during sampling we monitored pH to check for potential dissolved inorganic carbon (DIC) limitation. To avoid possible DIC limitation during high biomass periods, we added 200 µmol/kg bicarbonate together with equal amounts of HCl to buffer total alkalinity to the mesocosms. Bicarbonate was added on day 11 and day 15 to all mesocosms and on day 19 only to the most productive mesocosms (10 and 20 µM Si). The bicarbonate addition occurred together with the nutrient addition by adding $NaHCO_3$ and HCl to the canisters with the sample filtrate.

2.4 Sampling procedure

The experiment lasted for 3 weeks with the final sampling occurring on day 22. Throughout the experiment sampling activities occurred every second day, alternating with the nutrient additions, at 8:30 am, starting on day 0 prior to the first nutrient addition (Fig. 2a). Watercolumn samples were taken with a Kemmerer bottle from about 0.3m below the surface (Volume 6L, Wildco, Yulee, US). With 1 m length the sampling bottle integrated a large portion of the water column insider the mesocosms. Prior to sampling, the water column was mixed by moving the Kemmerer bottle up and down repeatedly. Due to the shallow depth of the mesocosms, the mesocosms represent a section of the water column that is naturally well mixed, as the spring MLD in Kongsfjorden is deeper than 5 m (Assmy et al., 2023; Hoppe et al., 2024). Thus, regularly mixing the mesocosms to

https://doi.org/10.5194/egusphere-2026-3186
Preprint. Discussion started: 18 June 2026

prevent stratification contributes to representing natural conditions. Subsamples for DIC, microscopy and nutrients were filled into 200 mL opaque PE bottles, carefully avoiding bubbles. The remaining water was transferred into 2x 10L sampling canisters. A total volume of 8 L was sampled from each mesocosm on regular sampling days. pH (826 pH mobile with a LL aquatrode plus pt1000, Metrohm) was measured immediately after sampling in the sampling containers. The sample containers were stored in the cold for a maximum of 2 hours until sample processing of particulate organic carbon (POC), nitrogen (PON), phosphorus (POP) and biogenic silica (BSi), as well as pigments and DNA. Every four days starting on day 2, additional 6 L were sampled for stable isotope primary productivity bioassays. The sediment trap was sampled in weekly intervals on days 7, 13 and 22 of the experiment. The sediment trap was emptied into a clear 2 L polycarbonate bottle by carefully removing the rubber plug at the bottom of the sediment trap. The samples were kept in the cool and dark until subsequent subsampling for POC/N and BSi. On day 7 the samples from the 2 and 5 µM Si mesocosms were lost during sampling. During the final sampling the accumulated sediment exceeded the volume of the sediment trap in the 10 µM Si mesocosm and the sediment was therefore not sampled fully.

2.5 Sample analysis

2.5.1 Carbonate chemistry

DIC samples were taken gas-free by filtering subsamples in triplicates (0.2 µm) and storing the samples upside down in gas-free Zinsser vials (1.8 mL) at 4°C until analysis. Analysis took place at MPI Bremen using the flow injection system (Hall and Aller, 1992) equipped with an autosampler (Spark Optimas 820, Spark, Netherlands).

Carbonate chemistry was calculated using pH and DIC as input variables using the CO2sys macro in Microsoft Excel (Pierrot et al., 2006). Seawater density to convert DIC and nutrient concentrations to µmol kg^{-1} was calculated using the seacarb package in R (Gattuso et al., 2026) applying surface (0-1 m during the upcast) salinity values obtained from the regular fjord monitoring at station KB3 on May 2 and May 6. pH was converted to total scale using 1°C as a target temperature. Carbonic acid thermodynamic equilibrium constants (K_1 and K_2) were based on (Lueker et al., 2000). K_f was based on (Perez and Fraga, 1987). $KHSO_4$ was based on (Dickson, 1990). DIC concentrations showed a drastic increase beyond what would be biologically reasonable on day 18 of the experiment. This increase coincided with the start of a new measurement run of DIC. While this suggests a possible methodological issue, standard calibration of this measurement day was in line with the other measurement days. Hence, the data can not be excluded, but the calculated carbonate chemistry on these days should be considered with lower confidence.

2.5.1 Particulate organic matter (POM)

For POC/N, POP and BSi analysis a subsample of up to 1L was filtered applying a gentle pressure of ~300 mBar. For POC/N and POP we used precombusted glass-fiber filters (GFF, ø25 mm, 0.7 µm nominal pore size, Whatman, UK) and for BSi analysis polycarbonate filters (ø47 mm, 2 µm pore size, Merck Millipore Ltd., Cork, Ireland) as well as a glass-free filtration

https://doi.org/10.5194/egusphere-2026-3186
Preprint. Discussion started: 18 June 2026

setup. All filters were frozen and stored at -20 °C until analysis in the home laboratory. There the filters for POC/PON were dried for 24 h at 60 °C, then acidified with 200 µL of 0.1M HCl and subsequently dried again. Afterwards POC/PON filter were wrapped in tin capsules and measured using a Euro EA3000 Elemental Analyzer (Eurovector, Pavia, Italy). POP filters were autoclaved for 30 min in 100 mL Schott Duran glass bottles using an oxidizing decomposition solution (Merck, catalogue no. 112936) to convert organic phosphate to orthophosphate. Phosphate concentrations were determined spectrophotometrically following (Hansen and Koroleff, 1999). Biogenic Silica (BSi) was measured following a modified procedure by (DeMaster, 1981) (Krause et al., 2023). Biogenic Silica (BSi) was analysed using an alkaline time-course digestion (0.1M Na_2CO_3) at 85°C in a water bath with subsampling at 0.5, 1, 2 and 3 h timepoints. This was followed by a 48 h hydrofluoric acid (2.0 M) digestion to dissolve the remaining lithogenic silica (LSi). Spectrophotometric analysis of the solubilized silica was conducted using a Thermo Scientific Genesys 10 UV–VIS Spectrophotometer (Thermo Fisher Scientific, Waltham, US). Model I linear regression was performed to calculate the concentrations of BSi while accounting for the amount of LSi that leached out during the alkaline digestion.

2.5.2 Photosynthetic pigments

For photosynthetic pigment analysis including Chl *a*, up to 1 L of water were filtered onto a glass-fiber filter (GFF, ø 25 mm, 0.7 µm nominal pore size, Whatman, UK) using a gentle vacuum of 300 mBar. Immediately after, the filters were placed in cryovials, and frozen at -80 °C until analysis of photosynthetic pigments using reverse-phase high-performance liquid chromatography (HPLC). Pigments for HPLC analyses were extracted in acetone (100 %) in plastic vials by homogenisation of the filters using glass beads in a cell mill followed by centrifugation (10 min, 5200 rpm, 4 °C) and filtration of the supernatant through 0.2 µm PTFE filters (VWR International). Phytoplankton pigment concentrations were determined in the supernatant by reverse-phase high-performance liquid chromatography (Thermo Fisher Ultimate 3000 with an Eclipse XDB-C8 3.5u 4.6 x 150mm) following (Van Heukelem and Thomas, 2001)

2.5.3 Dissolved inorganic nutrients

Upon arrival in the lab, water samples for inorganic nutrients were filtered (0.2 µm cellulose acetate syringe filter, VWR International, USA) and stored in the fridge in polypropylene tubes until analysis within 24 h. A second set of samples was filtered and frozen at -20 °C for analysis in the home laboratory. Both on site and in the home laboratory samples were analysed in duplicates. Dissolved inorganic nutrients (nitrate, nitrite, phosphate, dissolved silicic acid and ammonium) were analysed using a continuous flow analyzer (QuAAtro Autoanalyzer, SEAL Analytical, Norderstedt, Germany) connected to a fluorometer (FP-2020, JASCO, Tokyo, Japan) to measure ammonium. No ammonium was measured from frozen samples. On site and frozen samples were in good agreement (data not shown), hence on site measurements were used for analysis.

https://doi.org/10.5194/egusphere-2026-3186
Preprint. Discussion started: 18 June 2026

2.5.4 Carbon, nitrogen and silicon bulk uptake rates

The water sampled from the mesocosms for stable isotope bioassays was transferred immediately into duplicate 2L clear polycarbonate bottles for each mesocosm. Stable isotopes ^{13}C- sodium bicarbonate (99 %, Merck, Taufkirchen, Germany), ^{15}N-sodium nitrate (99%, Merck, Taufkirchen, Germany) and ^{30}Si-sodium metasilicate were dissolved in ultrapure water (MilliQ) to produce stock solutions. ^{30}Si-sodium metasilicate was produced by fusing enriched ^{30}Si- silicon dioxide (99 %, Neonest AB, Solna, Sweden) with anhydrous sodium carbonate (Merck, Taufkirchen, Germany) in a platinum crucible. Stable isotopes were added to one set of replicates. The other set was used as a control. ^{13}C-sodium bicarbonate was added at a 10 % enrichment level. ^{15}N-sodium nitrate was added as a fixed quantity of 0.5 µmol/L resulting in enrichments between 5 and 98% averaging 20±28 %. ^{30}Si-sodium metasilicate was added relative to the intended Si concentration in the mesocosms aiming for a 15% enrichment. In the Si depleted mesocosms the enrichment was up to 99% resulting in an average enrichment of 36±31%. The bottles were subsequently incubated for 24 hrs. On day 2 the incubation was conducted under in situ conditions by tying the bottles in the harbour next to the mesocosms. All subsequent incubations were conducted under simulated in situ conditions in the lab at 2°C with 80-90 µmol photons m^{-2} s^{-1} of light. At the end of the 24 hour incubation, the bottles were subsampled for ^{13}C-labelled dissolved inorganic carbon (^{13}C-DIC), ^{13}C and ^{15}N labelled POC and PON (^{13}C/^{15}N-POC/PON) and ^{30}Si labelled biogenic silica (^{30}Si-BSi). For ^{13}C/^{15}N-POC/PON 1 L of each bottle was filtered analogous to POC/PON onto precombusted GF filters (ø25 mm, 0.7 µm nominal pore size, Whatman, UK). The filters were frozen and stored at -20 °C. For analysis the filters were dried for 24 h at 60 °C then acidified with 0.5 mL of 0.1 M HCl and subsequently dried again. The dried filters were packed in tin capsules and measured with an IA-IRMS (get details for stockholm mass spec) against Pee Dee Belemnite and Air as a standard for carbon and nitrogen, respectively. Samples for ^{13}C-DIC analysis were taken from each incubation bottle after the incubation, by filtering (0.2 µm cellulose acetate syringe filter, VWR International, USA) and storing the samples upside down in 12 mL glass exetainers at 4°C in the dark until analysis. The samples were measured in duplicates using a Cavity Ring-down Spectrometer G2101-i (Picarro, Santa Clara, USA) at Groningen University by acidifying the samples with 1% phosphoric acid and purging with N_2 as a carrier gas (Bach et al., 2025).

For ^{30}Si-BSi 1L subsamples were filtered onto polycarbonate filters (2 µm, ø 47 mm; Merck Millipore Ltd., Cork, Ireland) using a glass-free filtration setup. The filters were frozen and stored in Eppendorf tubes at -20 °C. For analysis the filters were dried within the tubes for 36 h at 60 °C in a drying oven. Biogenic silica was analysed using a 30 min two-step alkaline digestion with 0.1M Na_2CO_3 following (Krause et al., 2023). For isotope analysis, a subsample of the digested BSi solution was diluted with deionized (18.2 MΩ resistivity, MilliQ brand) water to 100 ppb. Stable isotope composition of these subsamples was measured using a high-resolution sector field inductively coupled plasma mass spectrometer (Element XR; Thermo Fisher Scientific, Waltham, US) following (Fripiat et al., 2009).

Due to the intense bloom observed in the mesocosms, exponential growth was assumed when calculating C, N and Si uptake rates following (Bach et al., 2025) for C uptake:

$$\rho_C = ln\left(\frac{DIC_E - POC_0}{DIC_E - POC_E}\right) \times \frac{[POC_E]}{t} \quad (1)$$

https://doi.org/10.5194/egusphere-2026-3186
Preprint. Discussion started: 18 June 2026

using the percentage of ^{13}C in enriched (POC_E) and blank samples (POC_0) and the percentage of ^{13}C available in the DIC (DIC_E). Absolute C uptake rates (C) were calculated using the POC concentration of the enriched sample taken after incubation ($[POC_E]$). N and Si uptake were calculated using the same equation as established for ^{32}Si incubations from for Si uptake (Brzezinski and Phillips, 1997). Natural abundance ^{13}C, ^{15}N and ^{30}Si percentages were obtained from the literature for the Eurasian Arctic (Bauch et al., 2015, Thibodeau et al., 2017; Liguori et al., 2020). The enrichment in all samples exceeded 3 standard deviations of the respective blank. Because the tracer enrichment exceeded the recommended 10 %, indicating an over-enrichment of these compounds in natural environmental samples, these measurements more accurately reflect potential rather than *in situ* uptake rates. N and Si uptake rates were not corrected for isotope dilution effects (Elskens et al., 2007; Gilbert et al., 1982) and may therefore be underestimated. However, the errors would probably be small because of the short incubation times and slow N remineralization and Si dissolution rates at low temperatures (Baer et al., 2017; Brzezinski et al., 2001).

2.5.4 Single cell carbon, nitrogen and silicon uptake rates

At three timepoints throughout the experiment (day 6, 14 and 22) additional subsamples for single cell uptake analysis were taken from the primary productivity incubation bottles after the 24 h incubation.The samples were fixed with 2 % EM-grade paraformaldehyde (PFA; EMS, USA) for 24 h in the dark at 4 °C. Depending on the estimated biomass up to 40 mL of sample were filtered at a gentle vacuum of 100 mBar onto 2 µm pore size polycarbonate filters (ø 25 mm; Merck Millipore Ltd., Cork, Ireland) and washed three times with ~2-3 mL of phosphate-buffered saline (Merck Millipore Ltd., Cork, Ireland). The filters were then placed in plastic petri dishes, dried at room temperature and stored in the dark at 4 °C. (Sample preparation and analysis followed Thielecke et al., 2026) For analysis, representative subsections of each filter (~5x5 mm) were selected under a microscope, cut with a scalpel, and mounted on a glass plate. The filters were gold-coated with a 10nm layer. Single-cell ^{15}N and assimilation rates were determined by high resolution secondary ion mass spectrometry (HR-SIMS; IMS 1280, CAMECA, Gennevilliers, France) following (Halbach et al., 2025). Areas of interest were pre-sputtered with a primary Cs^+ ion beam of 3 nA for 120 s for diatoms and a beam of 200 pA for 30 s for flagellates over an area of 60 × 60 µm and then analysed with a 100 pA beam over 50 × 50 µm at a spot size of 1 µm for 50 cycles. Images were processed using the CAMECA WinImage2 software. Regions of interest were manually drawn around the algal cells. The $^{13}C/^{12}C$ and $^{15}N/^{14}N$ ratios were subsequently calculated as means across pixels for each region of interest. As no dedicated subsamples were taken for SIMS analysis from unenriched incubations, atom percentages from the unenriched bulk samples were used to establish enrichment thresholds: cells below blank + 25×SD for ^{13}C (1.15 At%) or blank + 3×SD for ^{15}N (0.426 At%) were considered unenriched. Individual cell measurements were grouped into three functional groups based on visual species classifications and Si content. Silicified cells were further distinguished from non-silicified taxa using a total Si signal threshold, which retained 95% of diatoms and 94% of flagellates while effectively discriminating functional groups: *Chaetoceros* spp. (n=841 cells), *Phaeocystis pouchetii* cf. flagellate forms (n=379), and small flagellates <5µm (n=104). Rare groups with <100 cells (dinoflagellates, choanoflagellates, ambiguous classifications) were excluded from subsequent analysis. Specific uptake rates (d^{-1}) for C and N

https://doi.org/10.5194/egusphere-2026-3186
Preprint. Discussion started: 18 June 2026

were calculated according to (Olofsson et al., 2019). Cell-specific carbon uptake (pg C cell^{-1} d^{-1}) was calculated by multiplying specific uptake rates by cell carbon content estimated from SIMS-derived biovolumes using (Menden-Deuer and Lessard, 2000) allometric equations (diatoms: POC = 0.288 × V^0.811; other protists: POC = 0.216 × V^0.939). Biovolumes were calculated from SIMS ROI area measurements using cylindrical geometry for diatoms (width:length = 0.5) and spherical geometry for non-diatoms. Molar uptake ratios (C:N, C:Si, Si:N) were calculated from specific uptake rates.

2.5.5 Phytoplankton community composition

Species composition was assessed by light microscopy and 18S rRNA metabarcoding. For phytoplankton community composition via light microscopy, a 50 mL subsample was taken from each mesocosm once per week and preserved with hexamine-buffered formaldehyde (1-2% final concentration), and stored in the dark at 4 °C until analysis. Microscopic analyses were conducted by settling between 3 mL and 10 mL of sample in an Utermöhl chamber (Utermöhl, 1958) and counting the different species with an inverted light microscope (Zeiss Axio Observer D1, Oberkochen, Germany). For sampling days 0 and 22 a different inverted light microscope was used (Zeiss Axiovert 135, Oberkochen, Germany). Identification to the lowest possible taxonomic level was based on available literature (Hoppenrath et al., 2009; Kraberg et al., 2010; Throndsen et al., 2007; Tomas et al., 1997).

For 18S rRNA metabarcoding, in the same filtration setup as described above, 0.5 to 1 L of sample was filtered on precombusted GFF filters (GFF, ø25 mm, 0.7 µm nominal pore size, Whatman, UK), stored in Eppendorf tubes and stored at -20°C until further analysis. The frozen filters were extracted using the NucleoSpin Soil extraction kit (Macherey-- Nagel GmbH, Germany) according to the manufacturer's protocol. Cell disruption by bead beating occurred twice for 30 sec each at 5 m/s using the FastPrep 5G (MP Biomedicals, Irvine, USA). Amplicon libraries of the V4 region (18S rRNA gene) were generated using the standard 16S Metagenomic Sequencing Library Preparation protocol (16S Metagenomic Sequencing Library Preparation, part no. 15044223 Rev. B. Illumina, United States) using the forward primer CCAGCASCYGCGGTAATTCC and reverse primer ACTTTCGTTCTTGAT. ena and sequenced on a NextSeq 2000 sequencer (Illumina, United States) using the NextSeq™ 1000/2000 P1 XLEAP-SBS™ Reagent Kit (Illumina, United States). Cutadapt (vXA) was used for processing of the FastQ sequence files to remove PCR primer matches. The 18S sequencing reads were analyzed using the following parameters: maxEE = c (2.2, 2.1), minLen= 150,truncLen = c (220, 210), minBoot = 70, and minOverlap=10 bases. To conduct 3'-end trimming, error filtering, sequence denoising, paired-end reads merging, chimera detection and removal, and the determination and annotation of Amplicon Sequence Variants (ASVs) we applied the DADA2 pipeline (v1.38 of the software package, (Callahan et al., 2016)) implemented in R v4.5.2 (R Core Team, 2025). The taxonomy was assigned using the reference database PR2v5.1.1 (González-Miguéns et al., 2025). 18S rRNA gene amplicon data were processed and analyzed using the phyloseq package in R. ASVs annotated as metazoans, bacteria and archaea were removed from the dataset. ASV counts were transformed to relative abundances at species level.

https://doi.org/10.5194/egusphere-2026-3186
Preprint. Discussion started: 18 June 2026

2.5.6 *Phaeocystis* quantification via dPCR

Because small flagellates are difficult to identify in light microscopy, introducing uncertainty regarding the quantitative estimation of *Phaeocystis* we complemented the microscopy analysis with a dye-based digital PCR (dPCR) assays for absolute quantification of *Phaeocystis* target-gene copies, without the need for standard curves, as previously investigated for HAB monitoring assays in Irish waters (Caputo et al., 2025). Primer sequences (82F-(5′-GTG AAA CTG CGA ATG GCT CAT-3′)/P1np(5′-CGG GCG GAC CCG AGA TGG TT-3′) were based on (Metfies et al., 2016). Assays were performed on the QIAcuity Four Digital PCR System (QIAGEN) with a 8.5k 96-well nanoplate. Amplification performance for the primer sequences was previously assessed using quantitative PCR (qPCR) assays. qPCR was conducted using five-point 10-fold dilution series and used environmental DNA extracts as templates for the dilution series, as no synthetic standards or reference cultures were available. qPCR methods and results of standard curves and melting curve analysis to assess assay performance and specificity are detailed in Text S2.

Following the manufacturer's recommendations, the PCR pre-mix was prepared in a final volume of 12 µL and then transferred into each well of the dPCR nanoplate. Maintaining the same reagent proportions used in the qPCR reactions, the reaction mixture contained 1× QIAcuity EvaGreen PCR Kit mastermix (QIAGEN), primers at a final concentration of 400 nM, 1.2 µL of DNA template, and molecular-grade water (Sigma-Aldrich, Steinheim, Germany). Prior to analysis, environmental DNA extracts were diluted 1:100 in molecular-grade water to prevent signal oversaturation and to maintain an appropriate target occupancy across partitions and ensure reliable Poisson-based quantification (Whale et al., 2020). In the absence of standardized positive controls, the same environmental DNA extracts used in the qPCR assays were employed as reference templates using sample A30. All samples, positive and NTC were run in technical duplicate. Amplification was performed according to the manufacturer's thermal protocol, using the following cycling conditions: an initial denaturation step of 2 min at 95 °C, followed by 40 cycles of 15 s at 95 °C, 15 s at 60 °C, and 15 s at 72 °C. Imaging settings for the green channel were set to 200ms exposure and gain 4, and data analysis was carried out using the proprietary software QIAcuity® Software Suite Version 3.2. The absolute number of target molecules was automatically determined by multiplying the estimated copies per partition, derived from Poisson statistics, by the total number of valid partitions in each well. Target concentration was subsequently calculated by accounting for the partition volume and dilution factors. Copy numbers were converted to abundances using genome copy numbers (n= 9) reported for *Phaeocystis globosa* (Chen et al., 2024). Because species-specific copy-number information for the target species *Phaeocystis pouchetii* was not available, converted cell abundances should be interpreted as approximate estimates.

2.5.7 Sediment Trap Flux Calculations and Statistical Analysis

Particle export fluxes were calculated from sediment trap samples collected at three intervals during the experiment (Days 0-7, 7-13, and 13-22). Total particulate organic carbon (POC), particulate organic nitrogen (PON), and biogenic silica (BSi) were quantified from subsamples of the homogenized trap material following the protocol described in Sect. 2.5.2. Fluxes were

https://doi.org/10.5194/egusphere-2026-3186
Preprint. Discussion started: 18 June 2026

calculated by dividing total trapped amounts by the trap collection area (1.1310 m², based on 1.20 m diameter) and the collection period duration. Linear regression was used to quantify the POC to BSi flux relationship across all samples, and time-stratified correlations were calculated separately for each sampling day to assess temporal changes in export coupling. Complete nitrogen and silicon mass balances were calculated following (Boxhammer et al., 2018). Budget equations tracked inputs (cumulative nutrient additions), changes in standing stocks (dissolved and particulate pools), sediment trap exports, and residual (unaccounted) fractions over the 22-day experiment. Export efficiency was defined as the percentage of added nutrients recovered in sediment traps.

2.5.8 Growth rate calculation

Instantaneous growth rates for particulate organic carbon (POC), particulate organic nitrogen (PON), biogenic silica (BSi), and chlorophyll *a* (Chl *a*) as well as from microscopy abundances and dPCR-derived copy number for the dominant taxa *Phaeocystis* were calculated for each Si treatment between consecutive sampling timepoints as:

$$\mu = [\ln(C\_t_2) - \ln(C\_t_1)] / (t_2 - t_1) \quad (2)$$

Exponential growth phases were identified from consecutive time windows (minimum 3 timepoints) based on the following criteria: (1) coefficient of determination (R^2) ≥ 0.85, (2) positive growth rate ($\mu > 0$), and (3) statistical significance ($p < 0.05$).

2.5.9 Statistics

Uptake and particulate organic matter dynamics indicated two distinct bloom phases. To quantify the transition point, we fitted a smoothing spline to daily mean time series of nitrate drawdown rate, carbon uptake rate, Chl *a* and POC and extracted local minima (pracma package, (Borchers, 2025)). Nitrate drawdown rate, carbon uptake rate, and POC consistently placed the inter-phase minimum between days 14 and 15, while chlorophyll *a* identified the minimum later at day 18. Potential effects of the employed Si gradient were assessed separately for the two bloom phases (day 1-14 and 15-22). One way ANOVA was used to test for differences between mesocosms where no direct Si effect was expected i.e. carbonate chemistry. Spearman rank correlations were employed to assess correlation with the Si treatment. Where appropriate, linear models were used to quantify the relationship with dSi concentration. R code for statistical analyses, and visualisations was in part generated with the assistance of generative AI (Claude, Anthropic); all code was reviewed and validated by the authors. All analyses were performed in R using the tidyverse package suite and ggplot for visualisations with significance threshold $\alpha = 0.05$ (R Core Team, 2025; Wickham, 2016; Wickham et al., 2019).

3. Results

3.1 Environmental conditions and carbonate chemistry

The experiment ran from May 4-26, 2024. Air and water temperatures rose during the first half of the experiment (water: 1.2 to 2.3°C), before dropping sharply following sea ice intrusion on day 15 (to -0.2±0.4°C) and glacial ice presence on day 21 (to

https://doi.org/10.5194/egusphere-2026-3186
Preprint. Discussion started: 18 June 2026

-0.8±0.3°C). Occasional snowfall after day 11 and ice caused temporary shading but no structural impact on the mesocosms. Light availability was consistently high (avg. 1211±1706 Lux), based on a comparison measurement with a PAR sensor on day 6, when 1956±1352 Lux corresponded to 155±46 µmol photons m^{-2} s^{-1}. Variability within individual mesocosms reflected diel and weather-driven fluctuation (CV ~60–150%). On average, mesocosms positioned toward the inside of the box received around 40% less light than the harbour control. This could indicate more persistent shading from harbour structures or mesocosm walls. However, this pattern matching the mesocosm location was not consistent across all mesocosms and could therefore also point to differences in sensor positioning inside the mesocosms.

Consistent with increasing biomass and carbon consumption in the mesocosms, pH rose gradually alongside declining DIC in the first half of the experiment. The subsequent bicarbonate additions prevented CO_2 from falling below 5 µmol kg^{-1} with the exception of mesocosms Si 20 on day 14 (4.2 µmol kg SW^{-1}). Carbonate chemistry was well controlled resulting in an average pH of 8.36±0.1 and average DIC of 2181±79 µmol kg^{-1}, while the HCl additions helped to maintain a stable total alkalinity (2466±108 µmol kg^{-1}).

3.2 Biomass accumulation and temporal bloom development

The repeated addition of nutrients led to the rapid development of a bloom across all mesocosms (Fig. 3). Particulate organic matter (POC, PON) and Chl *a* concentrations exhibited similar temporal dynamics across all Si treatments, characterized by exponential growth during days 3.5-10, peak concentrations between days 10-22 depending on treatment, followed by rapid decline after day 13.

https://doi.org/10.5194/egusphere-2026-3186
Preprint. Discussion started: 18 June 2026

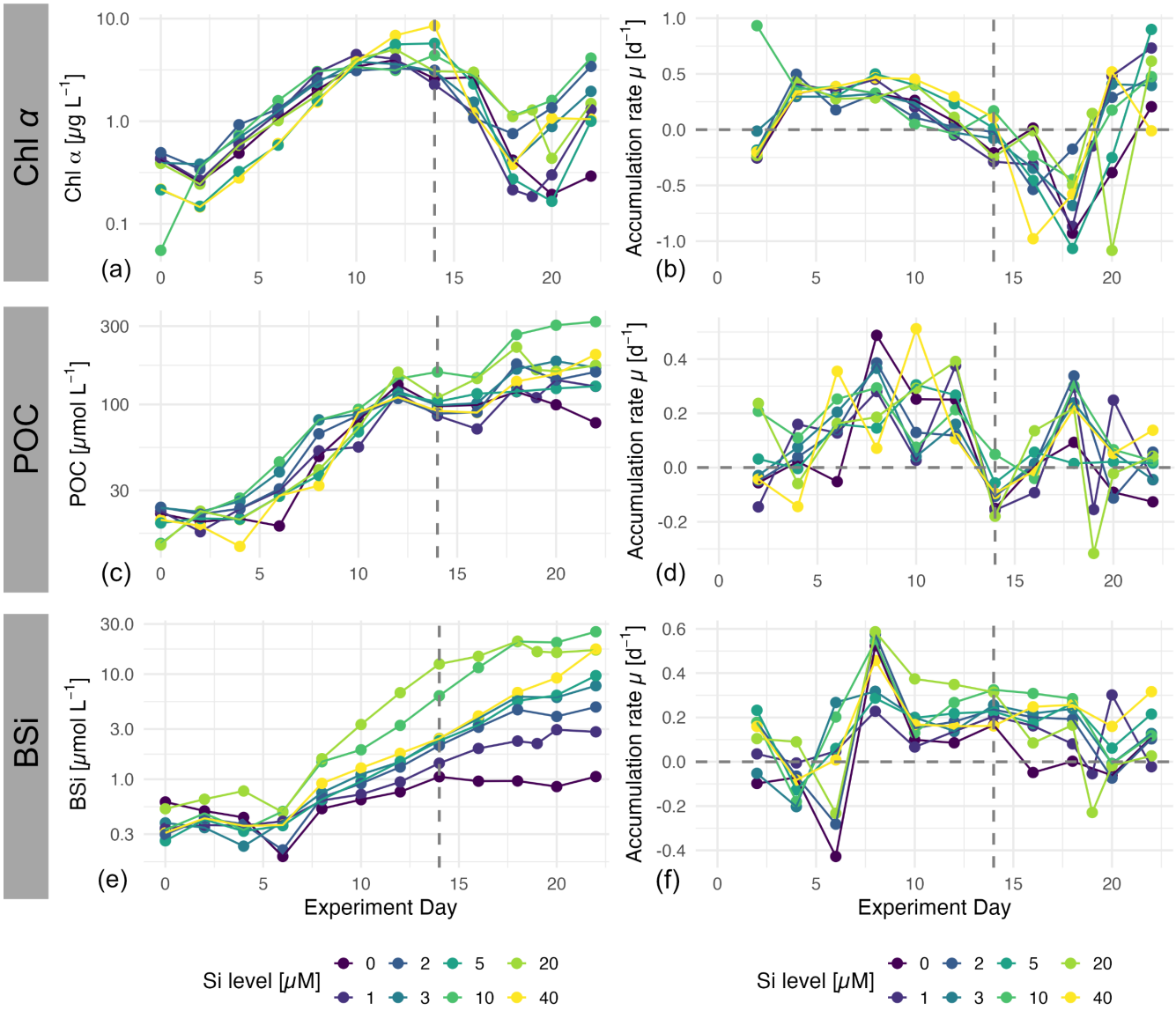

Figure 3: Temporal dynamics of particulate organic matter concentrations and biomass accumulation rates across Si treatments. Concentrations (left panels (a), (c), (e)) and accumulation rates (right panels (b),(d),(f)) for Chl *a* (top), particulate organic carbon (POC, center), and biogenic silica (BSi, bottom) over the 22-day experiment. Colours represent Si treatment levels from 0 to 40 µM. Concentrations are shown on $\log_{10}$ scale. Accumulation rates (µ, d^{-1}) were calculated as the instantaneous growth rate between consecutive timepoints, where positive values indicate biomass increase and negative values indicate biomass decrease. The vertical dashed line at day 14 indicates phase I and phase II of the bloom. Horizontal dashed lines at µ = 0 d^{-1} indicate zero biomass accumulation.

POC increased from initial concentrations of 14-24 µmol L^{-1} to maximum values ranging from 129-319 µmol L^{-1}, with exponential growth rates (µ) of 0.12-0.27 day^{-1} (mean phase duration: days 4.5-9.75, Fig. 4). Chl *a* showed earlier onset of exponential growth (mean start day 3.5, range: days 2-6, Fig. 4) with growth rates of 0.21-0.46 day^{-1}, increasing from 0.06-

https://doi.org/10.5194/egusphere-2026-3186
Preprint. Discussion started: 18 June 2026

0.49 µg L^{-1} to peak concentrations of 3.4-8.5 µg L^{-1} (Fig. 3a,b). Following peak biomass accumulation, both POC and Chl *a* exhibited declines starting on day 13, coinciding with the onset of widespread nitrogen and phosphate limitation, with Chl *a* showing a more severe decline in rates (µ = -0.29 to -1.07 day^{-1}) compared to POC (µ = -0.11 to -0.32 day^{-1}, Fig. 3b,d). In phase I of the experiment (day 0-14) Chl showed a correlation with Si treatments ($\rho = 0.7$, $p = 0.046$), while in phase II (day 15-22) that correlation was lost but POC and PON correlated with Si availability ($\rho = 0.74$, $p<0.05$ for both). In contrast, biogenic silica (BSi) displayed markedly different dynamics, with delayed exponential accumulation beginning around day 8 (range: days 8-14, Fig. 4) and continuing through day 15-18 with growth rates of 0.09-0.36 day^{-1} (Fig. 3f). BSi concentrations increased from 0.18-0.61 µmol L^{-1} to peak values of 1.1-25.3 µmol L^{-1}, with maximum concentrations strongly correlated with Si treatment level ($r = 0.63$, $p < 0.10$). Notably, BSi exponential growth persisted 3-7 days beyond the crash in POC and Chl *a*, and most high-Si treatments (≥10 µM) showed minimal BSi decline even through day 22, indicating continued silica frustule accumulation despite widespread phytoplankton mortality. The temporal succession from early Chl *a*/POC bloom (days 3-8) to delayed BSi accumulation (days 11-18) suggests an initial phase dominated by non-diatom growth, followed by a transition to diatom dominance that persisted through the nutrient-induced biomass crash. Across the entire experiment BSi was strongly correlated with Si availability ($\rho = 0.9$, $p<0.01$). POC:PON ratios were stable over time (11.4±0.6) although significantly higher than the Redfield ratio of 6.6, with the exception of the 10 and 20 µM Si treatments where the C:N ratios rose notably (13.6±1.7) following day 14. The Si:C ratio (analogous to Si:N) was stable initially at a low rate of 0.02±0.01 but increased throughout the experiment with a strong correlation with the Si gradient ($\rho = 0.93$, $p <0.001$) showing an accumulation of BSi relative to POC and PON with increasing Si availability.

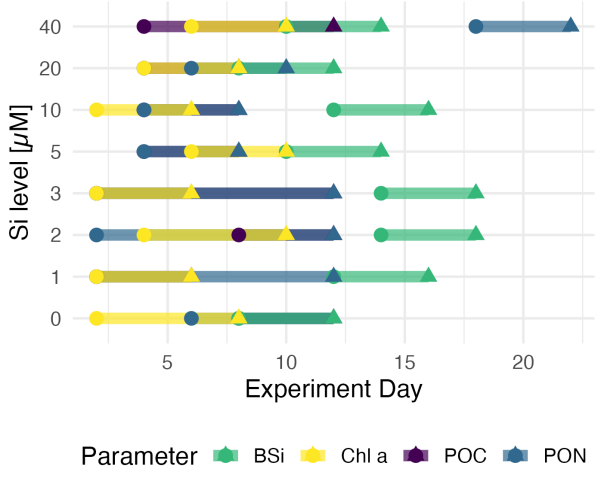

Figure 4. Temporal dynamics of exponential biomass accumulation across Si treatments and biomass parameters. Horizontal bars indicate the duration of exponential accumulation for each biomass parameter across Si treatment levels (0-40 µM). Exponential accumulation was defined as ≥3 consecutive timepoints with positive biomass accumulation rates. Circles mark the start of exponential growth, triangles indicate the end. Colors represent different biomass proxies: green = BSi, yellow = Chl *a*, purple = POC, blue = PON.

https://doi.org/10.5194/egusphere-2026-3186
Preprint. Discussion started: 18 June 2026

3.3 Community composition

The phytoplankton community underwent a two-phase succession pattern with *Phaeocystis* and *Chaetoceros* as the two main bloom species (Fig. 5 and A3). The early bloom phase (Days 0–14) was dominated by *Phaeocystis,* as supported by dPCR (Fig. A4)*,* which proliferated regardless of Si treatment, reaching peak abundances around Day 8–14 across all mesocosms, matching the Chl *a* development. Microscopy data show *Phaeocystis* (both single cells and colonies) reaching ~10^6–10^7 cells L^{-1} (10^5 cells L^{-1} based on dPCR), with colonies only present in significant abundances at the start of the experiment (Fig. 5). Correlation of dPCR and microscopy-based Phaeocystis abundances indicated good agreement regarding the temporal pattern of the bloom (Spearman rank, $\rho = 0.61$, $p<0.001$), despite differences in absolute abundance estimates. The lower estimates of *Phaeocystis* abundance from digital PCR compared to microscopy-based counts, likely reflect reduced DNA extraction efficiency from GF/F filters not originally intended for molecular analysis, in addition to possible systematic underestimation introduced by applying a genome copy number reported for *Phaeocystis globosa* (Chen et al., 2024), while microscopy-based counts upscaled from small counting volumes (3 mL) may overestimate true abundances. The 18S relative abundance data corroborate the *Phaeocystis* dominance, with *Phaeocystis* comprising 30–70% of reads in the early bloom period across most Si treatments. A transient minor bloom of *Micromonas polaris* developed towards the end of the early bloom phase (Fig. A3). A late bloom phase (Days 14–22) saw compositional shifts following the collapse of the *Phaeocystis* bloom contingent on Si availability: high-Si mesocosms (≥5 µM) developed diatom-dominated assemblages, dominated by *Chaetoceros* reaching ~10^8 cells L^{-1} in microscopy counts, with minor contributions from *Thalassiosira* spp. and different pennate diatoms. In contrast, low-Si treatments exhibited a more mixed community composed of *Chaetoceros*, dinoflagellates (*Gyrodinium* spp.) and flagellates (*Micromonas polaris*, unidentified small flagellates). Only in the 0 µM Si treatment *Chaetoceros* was no significant contributor at the end of the experiment (Fig. 5). Microscopy identified a higher contribution of *Chaetoceros* spp. in the low-Si treatment compared to 18S reads. *Grammonema striatulum* which emerged as a late-bloom taxon in 18S data could have been misclassified as *Chaetoceros* due to their ability to form chains of similar size to *Chaetoceros* contributing to this observed difference. In addition, the 18S data suggested substantial dinoflagellate representation throughout (particularly *Gyrodinium* spp. at 20–60% relative abundance in late bloom, Fig. A3), which appears disproportionately high relative to microscopy cell counts where dinoflagellates remain numerically subdominant to diatoms in high-Si treatments. This likely reflects high rRNA gene copy numbers in dinoflagellates (often 100–10,000+ copies per cell) inflating their proportional representation in 18S data (Liu et al., 2021; Martin et al., 2022).

https://doi.org/10.5194/egusphere-2026-3186
Preprint. Discussion started: 18 June 2026

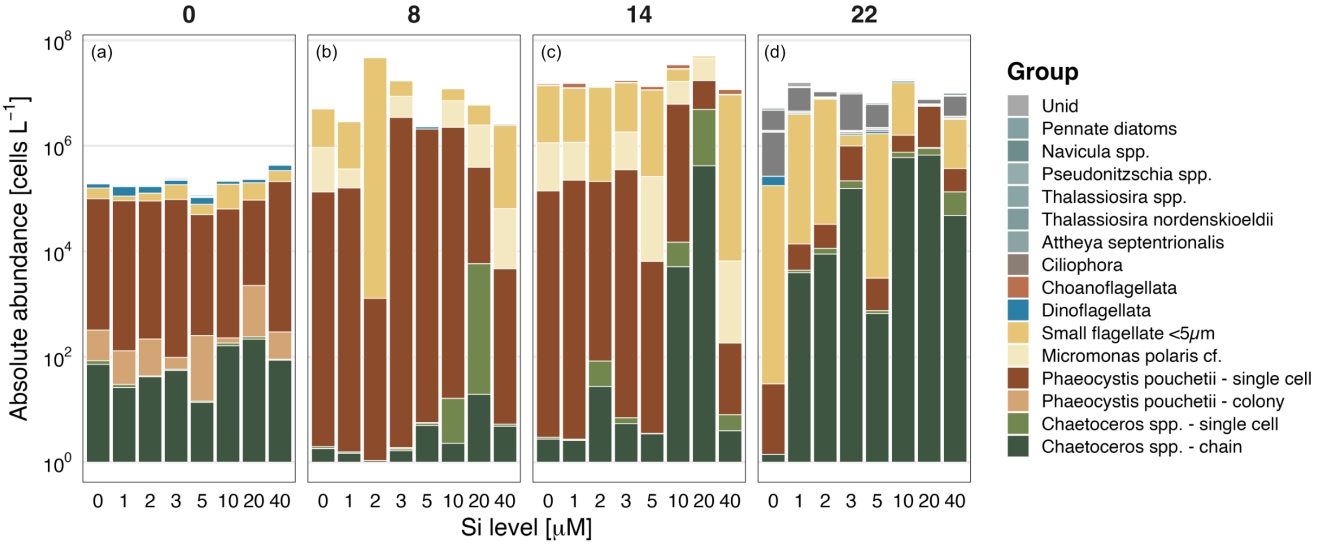

Figure 5: Composition and abundance (in cells L^{-1}) over time based on microscopy. Panels (a-d) represent experiment days.

3.4 Nutrient limitation

Nutrient drawdown between additions resulted in transient limitation events with distinct patterns across the Si gradient matching the observed biomass accumulation (Fig. 6). Limitation for phytoplankton growth was defined based on literature thresholds as 2 µM dSi, 0.1 µM phosphate and 1 µM nitrate (Downes et al., 2021; Egge and Aksnes, 1992; Lewis et al., 2019). The low Si treatments (0-2 µM) were below the defined threshold throughout the experiment. The 3 and 5 µM treatments first crossed the threshold on days 12 and 20 respectively, and the 10 µM treatment experienced brief Si limitation only during days 17-21. High Si treatments (20 and 40 µM) never experienced silicate limitation throughout the 22-day experiment. In contrast, phosphate limitation (< 0.1 µM) occurred episodically across all eight mesocosms with first crossings ranging from day 8-11, and reaching all mesocosms on day 12 (Fig. 6). Periodic nitrate limitation (< 1 µM) between additions similarly affected all mesocosms, first appearing on day 7 in the 2, 3, and 10 µM Si treatments, and peaking on day 11 when all mesocosms except the 40 µM treatment fell below the 1 µM nitrate threshold.

https://doi.org/10.5194/egusphere-2026-3186
Preprint. Discussion started: 18 June 2026

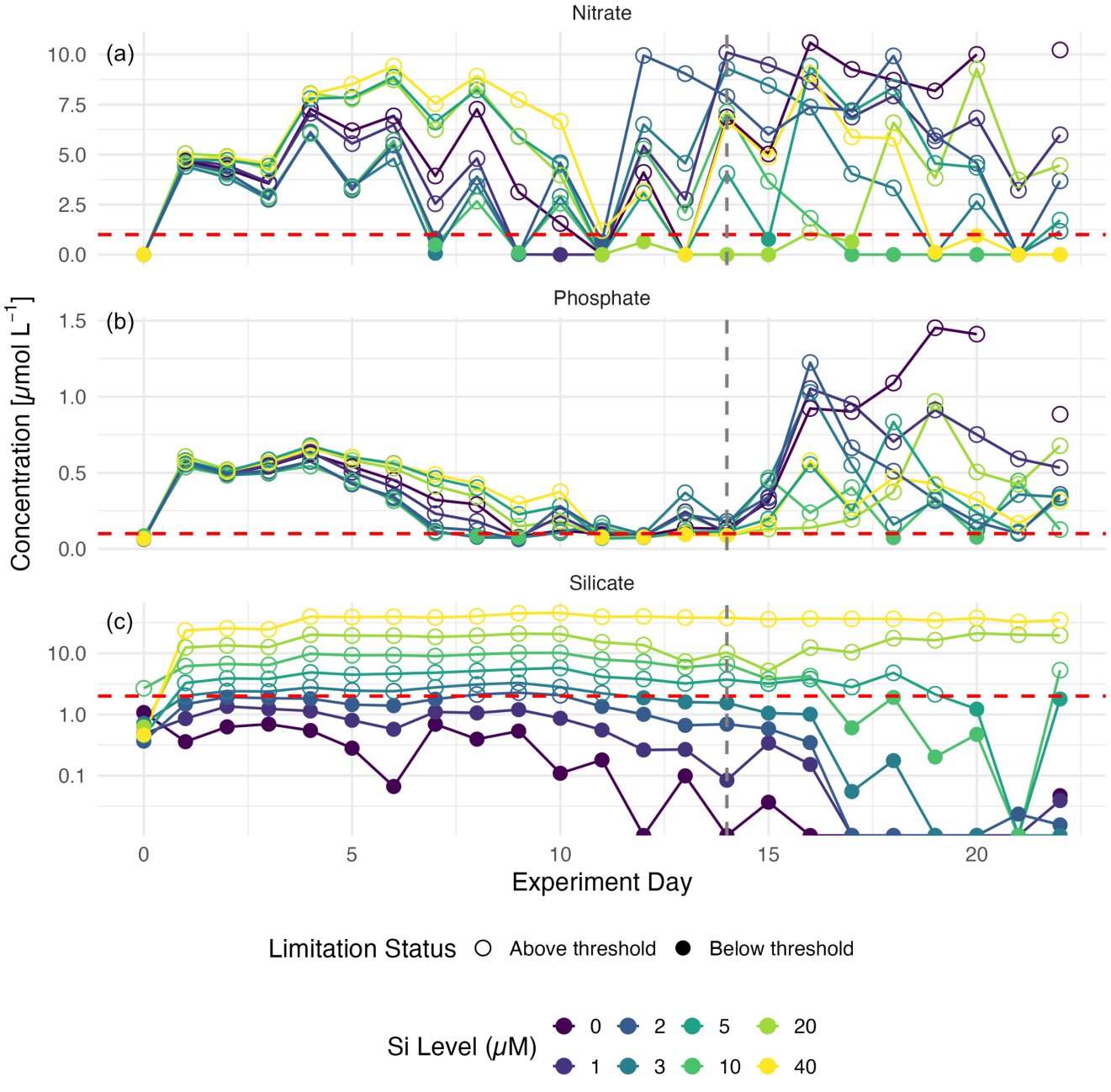

Figure 6: Development of nutrient availability for nitrate (a), phosphate (b) and silicate (c) in the mesocosms over time. Samples taken immediately after the nutrient addition were excluded. Red dashed line indicates limitation thresholds (1 µmol L^{-1} nitrate, 0.1 µmol L^{-1} phosphate, 2 µmol L^{-1} Si). Si concentrations are shown on a log scale to allow visual separation of low Si concentrations.

https://doi.org/10.5194/egusphere-2026-3186
Preprint. Discussion started: 18 June 2026

3.5 Nutrient drawdown and uptake

Nitrate drawdown rates (reported for the day following the nutrient addition) indicated two main bloom phases with minimum average nitrate drawdown on day 14 (Fig. 7). During the initial phase of the experiment nitrate drawdown rates increased exponentially from 0.9±0.4 µmol N L^{-1} to 6.9±2.2 µmol L^{-1}, mirroring phytoplankton growth peaking on day 9 to 11. The following days there was a strong decrease of nitrate drawdown until day 15. This early bloom phase was consistent across all mesocosms regardless of dSi treatment. The exception was mesocosm Si 20 where the peak lasted until day 15. Towards the end of the experiment nutrient drawdown rates picked up again reaching similar or even higher drawdown rates in some mesocosms compared to the early bloom phase (average 7.0±3.2 µmol N L^{-1} on day 21). Phosphate drawdown initially increased across all mesocosms, but then showed significantly higher variability especially following the crash of the Phaeocystis bloom after day 14 (average P drawdown of 0.4±0.2 µmol P L^{-1}). Si drawdown showed a contrasting pattern matching the pattern in BSi concentration, with Si drawdown rates increasing from 0.15±0.09 µmol Si L^{-1} to >4 µmol Si L^{-1} in the high Si treatments in the later phase of the experiment (Fig. 7c).

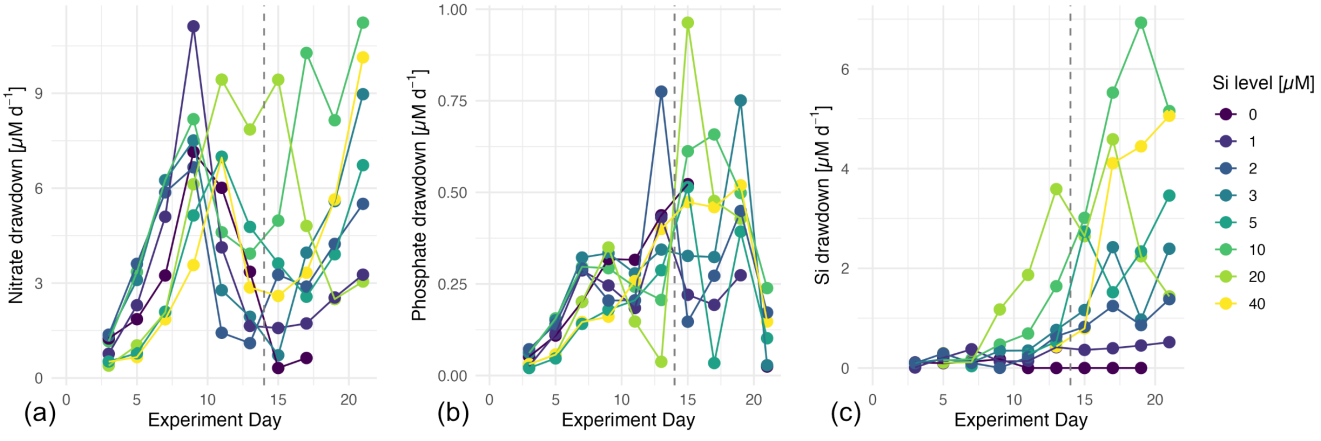

Figure 7: Nutrient drawdown rates of nitrate (a), phosphate (b) and silicic acid (c) for the Si treatments over the duration of the experiment. Drawdown rates were calculated only for the 24 h following each nutrient addition. Vertical grey lines separate phase I and II of the bloom.

During the early bloom phase (Days 1-14), nutrient drawdown rates showed no significant relationship with Si availability for any measured nutrient (Spearman correlation: $p > 0.16$ for all nutrients; $n = 48$). However, by the late bloom phase (Days 15-22), strong positive correlations emerged between Si levels and drawdown rates for silicate ($\rho = 0.796$, $p < 0.001$), nitrate ($\rho = 0.589$, $p < 0.001$), and phosphate ($\rho = 0.437$, $p = 0.012$; $n = 32$). For the low Si concentration range (0-10 µM), linear models explained substantial variance in Si drawdown ($R^2 = 0.85$, $p < 0.001$) and moderate variance in nitrate drawdown ($R^2 = 0.60$, $p < 0.001$), while phosphate drawdown showed weaker linear relationships ($R^2 = 0.26$, $p = 0.012$). Beyond 10 µM Si, no further increase in nutrient drawdown was observed.

Patterns in nutrient uptake rates generally matched the patterns observed in nutrient drawdown rates. Both C and N uptake rates followed a two phase pattern. In the early phase C uptake increased from 0.45 to up to 45 µmol L^{-1} on day 10 (0.01 - 3.2

https://doi.org/10.5194/egusphere-2026-3186
Preprint. Discussion started: 18 June 2026

µmol N L^{-1}). Following a drop in uptake rates on days 14 they increased again reaching up to 67 µmol C L^{-1} and 2.4 µmol N L^{-1}, respectively. Si uptake rates were low throughout the experiment in mesocosms receiving up to 3 µm Si. In the high Si mesocosms (5-40 µM Si) Si uptake rates increased over time reaching up to 6.6 µmol Si L^{-1} in the 10 µM Si mesocosm. Analogous to nutrient drawdown rates, carbon and nitrogen uptake showed no relationship to Si availability ($p > 0.50$ for both) in phase I (Fig. 8). However, silicate uptake rates correlated positively with Si treatment levels ($\rho = 0.78$, $p < 0.001$, $n = 32$). In phase II (Days 15-22), consistent with Si drawdown rates, Si uptake exhibiting a very strong correlation with Si treatment ($\rho = 0.98$, $p < 0.001$, $n = 16$). We also observed a significant correlation of C uptake rates ($\rho = 0.44$, $p < 0.001$), which increased with Si treatment between 0 and 3 µM Si, but did not increase further at Si concentrations exceeding 3 µM, while there was no correlation between N uptake rates and Si availability. In agreement with the drawdown rates a linear model was used to describe silica uptake in phase I ($R^2 = 0.68$, $p < 0.001$) and phase II ($R^2 = 0.76$, $p<0.001$). For nitrogen, isotope uptake rates were consistently lower than drawdown rates across both phases, corresponding to mean uptake:drawdown ratios of 0.28 ± 0.10 in phase I and 0.38 ± 0.25 in phase II (Fig. 8). This indicates that isotope incubations, conducted as 24-hour measurements at the midpoint between nutrient additions under progressively depleted conditions, captured 28-38% of the net nitrogen consumption measured over the 24 hours immediately following the nutrient addition. This was supported by silicate uptake vs drawdown patterns. In phase I, Si uptake:drawdown ratios from 0.71 to 3.36 (excluding treatments with near-zero drawdown). This reasonable agreement reflects that the Phaeocystis-dominated communities did not cause significant Si drawdown resulting in comparable measurements for the day after the nutrient addition (drawdown) and 24 hours later (uptake). In phase II, uptake:drawdown ratios converged to lower values (0.14-1.94) as the growing diatom population increasingly depleted silicic acid within 24hrs after addition.

Stoichiometric analysis of nutrient consumption revealed distinct patterns between uptake and drawdown measurements, with important deviations from Redfield ratios (C:N = 6.625, N:P = 16, N:Si = 1 for diatoms). Drawdown-based N:P ratios averaged 20.1 ± 10.1 in phase I and 16.0 ± 14.8 in phase II, both slightly elevated relative to Redfield expectations. In contrast, N:Si drawdown ratios showed marked phase- and treatment-dependent variation: Phase I ratios were consistently elevated (mean 19.8 ± 11.9, range 4.4-36.7), particularly at low Si treatments (0-5 µM: 26.6 ± 10.6), reflecting *Phaeocystis*-dominated communities with low Si demand. Phase II N:Si ratios declined substantially (mean 2.8 ± 1.4, range 1.5-5.2), converging toward diatom-typical values as *Chaetoceros* populations established, though remaining 2-3× higher than the 1:1 Redfield ratio expected for pure diatom assemblages (Brzezinski, 1985). Isotope uptake measurements showed contrasting patterns: C:N ratios averaged 11.6 ± 3.9 in phase I and 16.2 ± 5.1 in phase II, both substantially elevated above Redfield (6.625), suggesting N-limitation during the 24-hour incubation periods. N:Si uptake ratios in phase I (mean 5.2 ± 8.8) were considerably lower than N:Si drawdown ratios (19.8 ± 11.9), reflecting the isotope method's reflection of the N limitation 48 hours post nutrient addition. Phase II N:Si uptake ratios showed extreme treatment dependence (0.1-15.7), with low values at high Si treatments (10-40 µM: 0.2-0.3) indicating Si-replete diatom uptake, and elevated values at very low Si treatments (0-2 µM: 1.7-15.7) likely reflecting higher abundances of non-diatoms under Si-limited conditions.

https://doi.org/10.5194/egusphere-2026-3186
Preprint. Discussion started: 18 June 2026

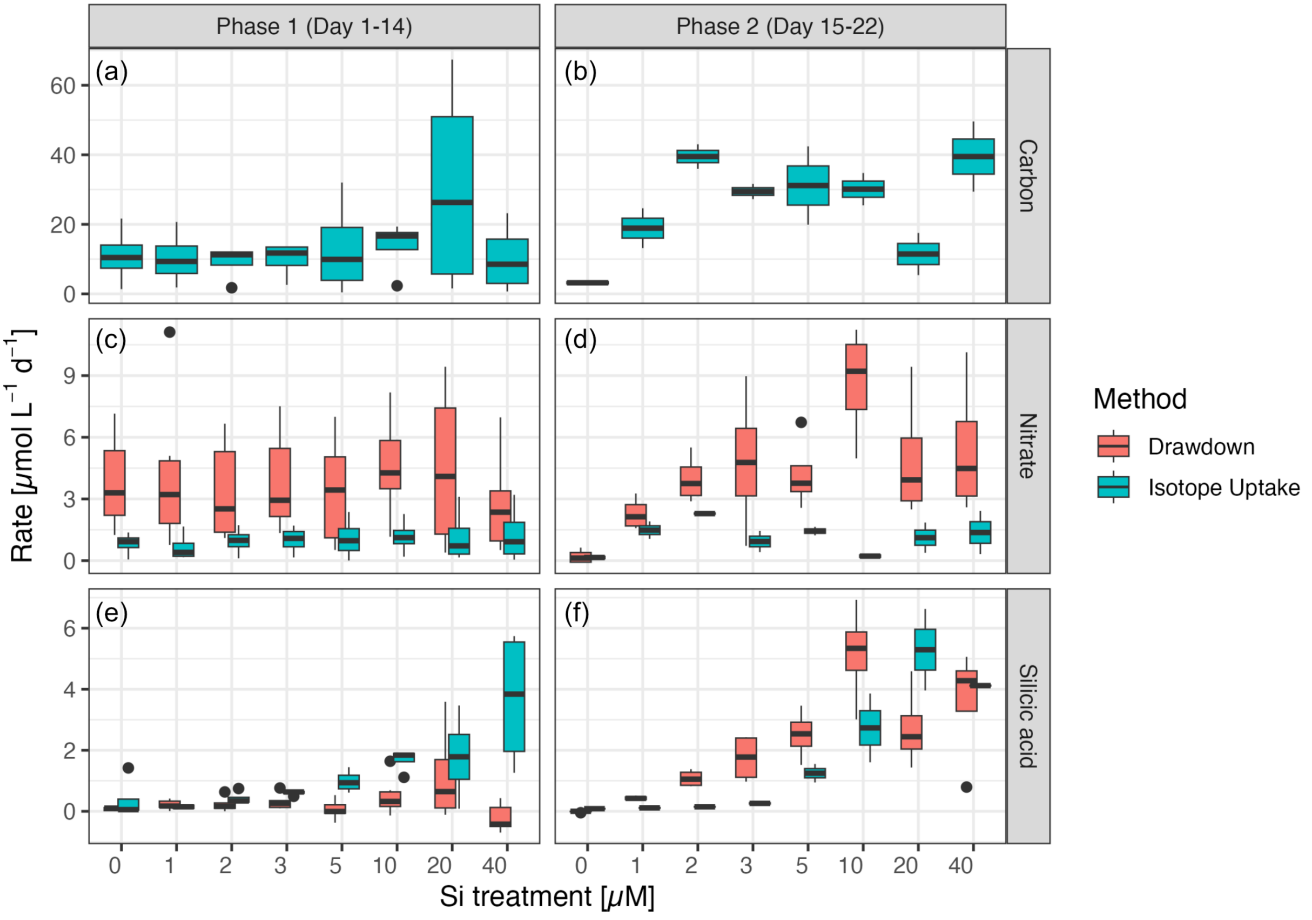

Figure 8: Comparison of uptake and drawdown rates across the two bloom phases and Si treatments. Boxplots showing carbon (top), nitrate (center) and silicic acid (bottom) rates during phase I (Day 1-14, left) and phase II (Day 15-22, right) across Si treatment concentrations (0-40 µM). Red boxes represent drawdown rates (net nutrient depletion on days following nutrient additions), while blue boxes represent isotope uptake rates. Sample sizes per Si level: Phase I drawdown n = 6, uptake n = 4; Phase II drawdown n = 4, uptake n = 2.

3.6 Export fluxes and N and Si mass balances

Overall, export efficiency was low (<15% based on nitrogen budgets), but export fluxes increased substantially by Day 22 across all Si treatments, with POC export ranging from 447 µmol m^{-2} d^{-1} (0 µM Si) to 2132 µmol m^{-2} d^{-1} (20 µM Si, Fig. 9a). Particle export fluxes from days 7, 13 and 22 showed strong coupling between BSi and POC export fluxes across all treatments and time points (Pearson $r = 0.858$, $p < 0.001$; linear model $R^2 = 0.735$), indicating diatom-dominated export throughout the experiment (Fig. 9c). The POC:BSi molar ratio of exported material declined progressively over time (Day 7: 21.2, Day 13: 5.63, Day 22: 2.58), reflecting increasing diatom contribution during bloom succession. High Si additions (≥20 µM) drove disproportionate BSi export during late bloom (Day 22: 194–628 µmol m^{-2} d^{-1}), demonstrating Si control over diatom export flux magnitude (Fig. 9b). The declining N:Si ratio in exported material (Day 7: 4–6; Day 22: 0.5–1.5) further confirmed the

https://doi.org/10.5194/egusphere-2026-3186
Preprint. Discussion started: 18 June 2026

increasing dominance of diatoms in particle export, consistent with a shift from *Phaeocystis*-dominated to diatom-dominated (*Chaetoceros*) community composition under Si enrichment. Export stoichiometry (C:N ratios: 5.85–9.49) remained relatively constant across treatments, suggesting limited impact of Si availability on the organic matter composition of exported particles despite the strong effect on BSi flux.

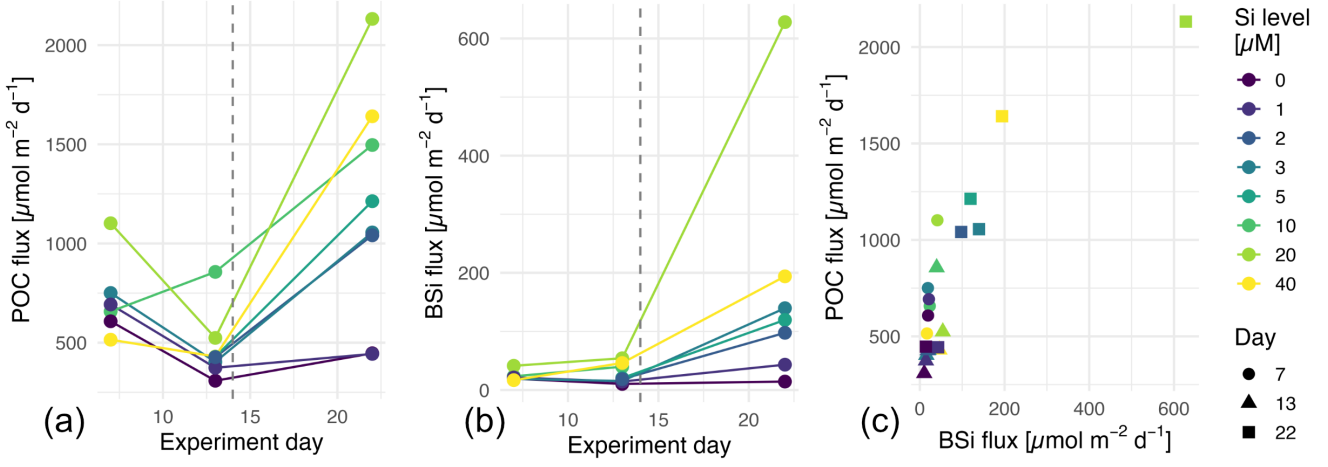

Figure 9: Export flux dynamics of POC (a) and BSi (b) over time. Correlation of POC and BSi flux (c) suggests tight coupling of total export flux to diatom contribution.

Nitrogen and silicon mass balances revealed contrasting patterns across the Si gradient. Nitrogen budgets showed 66–84% of added N remained unaccounted for in measured pools (dissolved DIN, particulate PON, and sediment trap export), with budget closure improving significantly at higher Si additions (−0.30% residual per µM Si added, $p = 0.048$, $R^2 = 0.50$, Fig. 10b). Nitrogen export efficiency increased strongly with Si availability, ranging from 5.6% of added N exported at Si0 to 15.2% at Si20 (+0.23% per µM Si, $p = 0.006$, $R^2 = 0.75$), demonstrating enhanced coupling between nutrient inputs and particle export under Si-replete conditions. Silicon budgets showed significantly higher budget closure (13–48% unaccounted, excluding 0 µM Si, Fig. 10a), with no significant Si gradient effect on budget closure ($p = 0.17$) or export efficiency ($p = 0.20$). Low Si treatments (1-3 µM Si) exhibited high Si export efficiencies (38–72%), while high Si treatments (10-40 µM Si) retained most added Si in dissolved or particulate pools with minimal export (3–28%), suggesting non-linear relationships between Si availability, frustule production, and BSi dissolution dynamics.

https://doi.org/10.5194/egusphere-2026-3186
Preprint. Discussion started: 18 June 2026

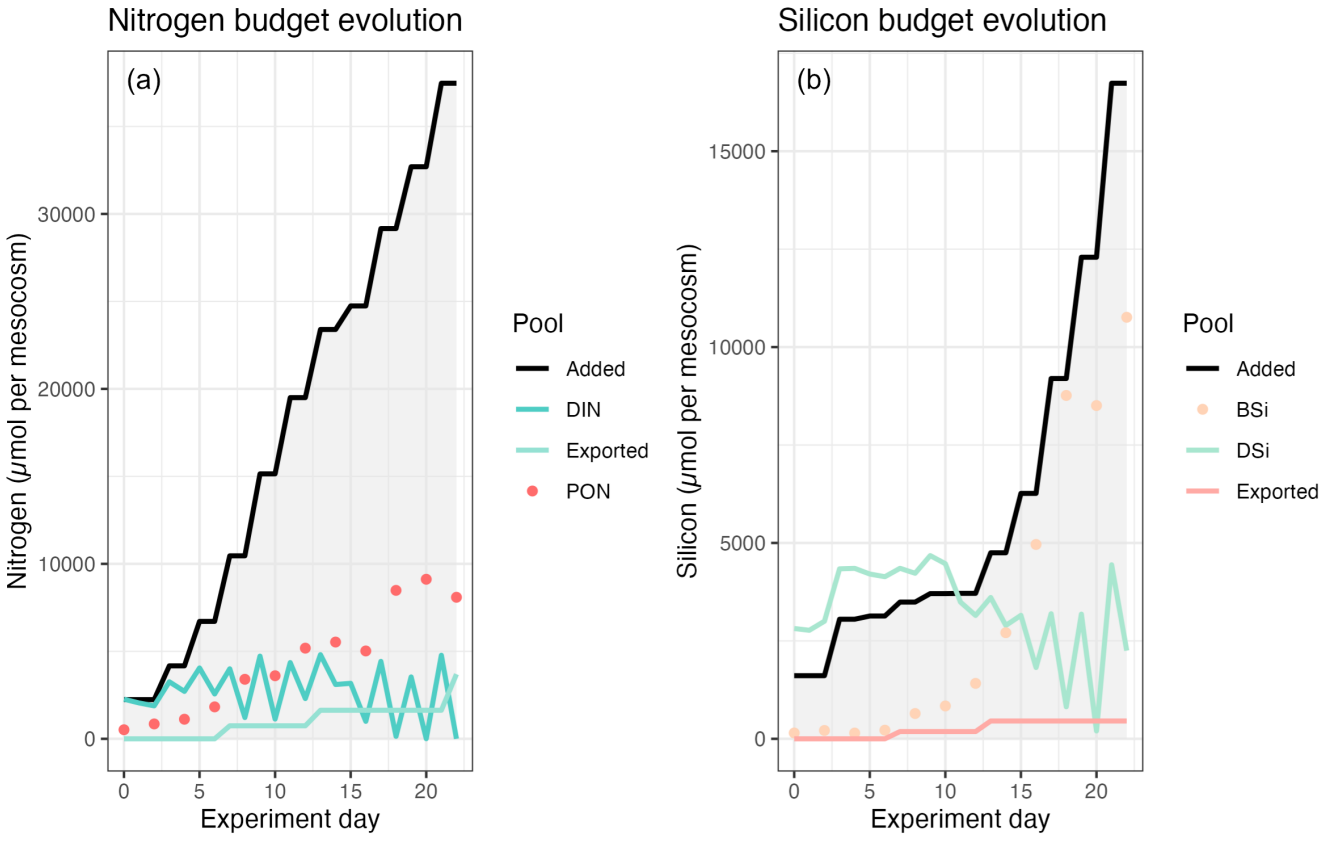

Figure 10: Exemplary budget evolution in the 10 µM Si mesocosm of dissolved, particulate and exported pools for nitrogen (a) and silicon (b) over time.

3.5 Species-specific biomass and uptake dynamics of *Phaeocystis* and *Chaetoceros*

Microscopy data was used to compare seed stocks of *Chaetoceros* and *Phaeocystis* and species-specific accumulation rates were calculated from cell counts and dPCR-derived genome copy numbers. At the start (Day 0), biovolumes were similar between species (*Chaetoceros*: $3.6 \times 10^7 \pm 1.7 \times 10^7$ µm³ L⁻¹; *Phaeocystis*: $3.4 \times 10^7 \pm 1.4 \times 10^7$ µm³ L⁻¹, mean ± SD; Wilcoxon rank-sum test, W = 36, p = 0.72), reflecting comparable seed stock densities.

Chaetoceros and *Phaeocystis* exhibited fundamentally different biomass accumulation dynamics throughout the experiment (Fig. 11). During the early exponential phase (Day 0–8), *Phaeocystis* grew approximately twice as fast as *Chaetoceros* (μ = 0.43 ± 0.15 d^{-1} vs. 0.22 ± 0.14 d^{-1}). The competitive balance reversed during the mid-growth phase (Day 8–14), when *Chaetoceros* sustained high accumulation rates (μ = 0.33 ± 0.11 d^{-1}), while *Phaeocystis* accumulation declined substantially (μ = 0.08 ± 0.14 d^{-1}). This shift coincided with nutrient depletion and the resulting collapse of the *Phaocystis* bloom. By the late phase (Day 14-22), *Phaeocystis* populations collapsed universally across all eight Si treatments (100% negative growth

https://doi.org/10.5194/egusphere-2026-3186
Preprint. Discussion started: 18 June 2026

rates, mean μ = -0.26 ± 0.06 d^{-1}). In contrast, *Chaetoceros* populations slowed but remained predominantly viable (μ = 0.04 ± 0.20 d^{-1}), being comparable to those of Phaeocystis during the transition between phase I and II.

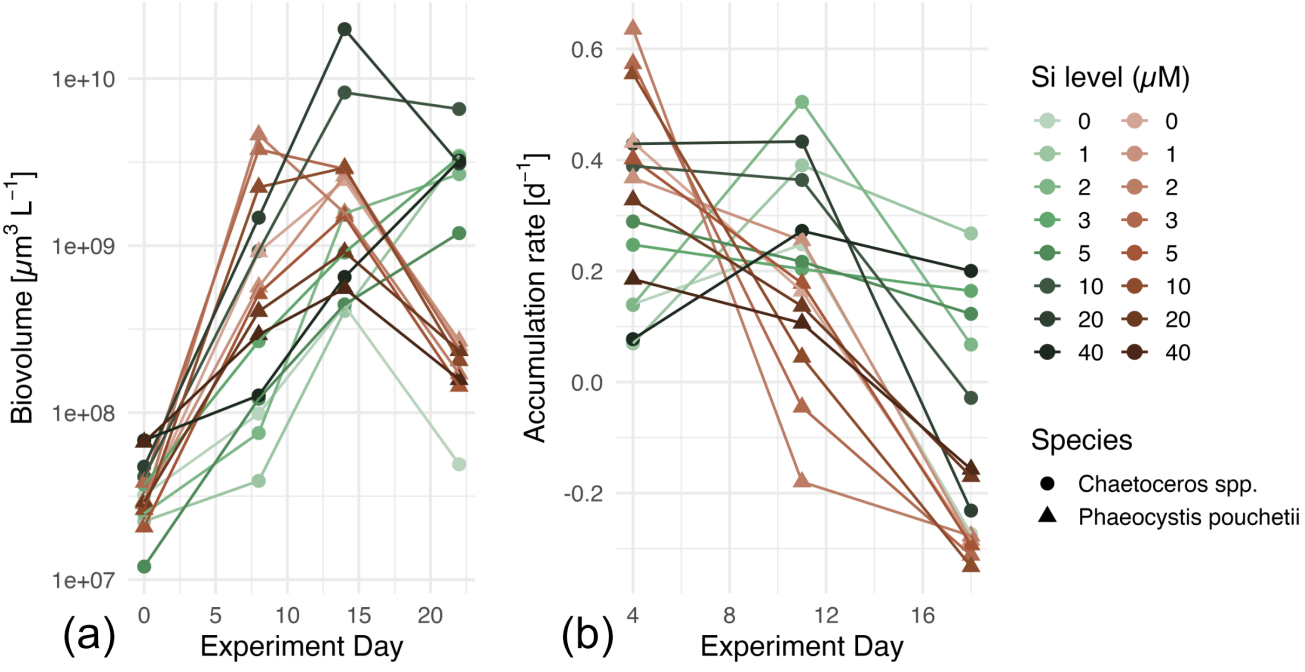

Figure 11: Species-specific development of biomass (a) and calculated accumulation rates (b) over time comparing *Phaeocystis* (green circles) and *Chaetoceros* (red triangles). Biovolume is displayed on a log scale to allow comparison of *Chaetoceros* and *Phaeocystis* at low abundances.

Single cell carbon and nitrogen uptake rates revealed contrasting temporal dynamics and Si sensitivities across phytoplankton groups. All three groups—*Chaetoceros* spp., *Phaeocystis pouchetii* cf., and small flagellates <5μm—exhibited similar early bloom C and N uptake rates during exponential growth (Day 6), but diverged substantially thereafter (Fig. 12). *Chaetoceros* showed gradual decline through mid- and late bloom phases, but maintained measurable activity throughout the experiment, while *Phaeocystis* and small flagellates crashed precipitously by Day 14, reaching near-zero uptake by Day 22. Stoichiometric ratios across all groups shifted from strongly N-enriched uptake (C:N < 1.1, well below the Redfield ratio of 6.6) during early bloom toward Redfield or C-enriched ratios by late bloom, with *Phaeocystis* exhibiting extreme C:N enrichment and high variability indicative of potential N stress. Si gradient effects on C uptake varied significantly across bloom phases. *Chaetoceros* showed minimal Si sensitivity during early bloom. At the critical mid-bloom phase (Day 14), *Chaetoceros* exhibited a non-monotonic Si response with optimal C uptake at intermediate Si concentrations and inhibition at high Si (64% reduction at Si 20 μM vs. optimal Si 3 μM, $p < 0.001$).

https://doi.org/10.5194/egusphere-2026-3186
Preprint. Discussion started: 18 June 2026

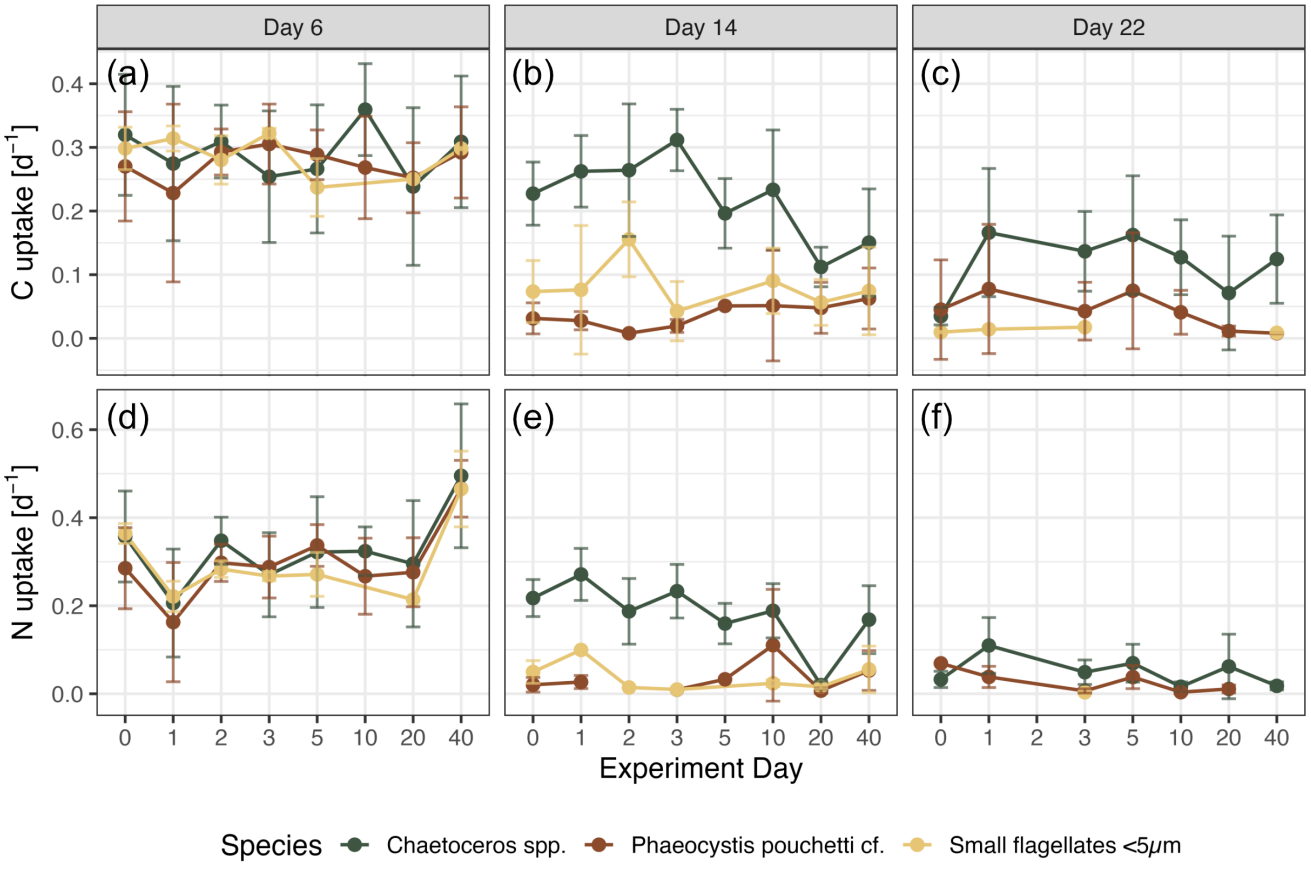

Figure 12: Mean single cell carbon (top) and nitrate uptake rates (bottom) of *Chaetoceros* spp (green), *Phaeocystis pouchetti* cf (red) and small flagellates (yellow) on three consecutive sampling days.

4. Discussion

4.1 Competition of *Phaeocystis* and *Chaetoceros* under varying Si concentrations

Despite similar seed populations of *Phaeocystis* and *Chaetoceros,* a bloom of *Phaeocystis* developed rapidly in our mesocosms regardless of Si supply. This *Phaeocystis* bloom collapsed around day 14 of the experiment and was succeeded by a diatom bloom. The second bloom was dominated by the chain-forming diatom *Chaetoceros spp.* indicated by the strong increase in BSi and confirmed by microscopy. In terms of nutrient drawdown as well as bulk uptake rates (Fig. 7) the second bloom reached a comparable intensity to the initial bloom although biomass accumulation (in terms of Chl a) had not yet reached a comparable magnitude at the end of the experiment (Fig. 3). In this second phase diatom biomass (based on BSi concentrations) showed a linear response to Si availability. The development of the initial *Phaeocystis* bloom regardless of the concentration of Si available challenges the perspective that Si availability is a key driver in deciding *Phaeocystis* vs diatom blooms (Ardyna et al., 2020; Dąbrowska et al., 2025) and confirms previous observations that Si concentrations limiting for diatoms are not a

https://doi.org/10.5194/egusphere-2026-3186
Preprint. Discussion started: 18 June 2026

prerequisite for *Phaeocystis* bloom development (Assmy et al., 2023; Hoppe et al., 2024; Peperzak et al., 1998). Phytoplankton bloom development is a function of initial population density (seed stock) and integrated growth rates over time. While microscopy-based abundances demonstrate comparable seed populations for both species, biomass accumulation within the first week was on average higher in *Phaeocystis* compared to *Chaetoceros* as suggested by microscopy. To explore nutrient consumption of diatoms compared to *Phaeocystis*, we applied a fixed Si:N ratio of 1.85 for Arctic diatoms based on conversion from (Lomas et al., 2019) to the nitrate and Si drawdown rates. Diatoms were responsible for less than 10% of nitrate drawdown until day 10, showing significantly higher nitrogen use by non-diatoms, which were dominated by *Phaeocystis* at the time, supporting field observations of rapid and efficient nitrate drawdown by *Phaeocystis* (Assmy et al., 2023). Net growth is determined by bottom-up processes (temperature, light and nutrients) and mortality controlled by top-down processes (pathogens, parasites and grazing). In the following we will discuss the potential contribution of each of these factors on *Phaeocystis* vs *Chaetoceros* growth.

The initial accumulation rates based on microscopy of *Phaeocystis* are higher compared to *Chaetoceros* ($\mu = 0.43 \pm 0.15$ d^{-1} vs. 0.22 ± 0.14 d^{-1}, respectively, Fig. 11). In general, these accumulation rates are within the range of growth rates reported in the literature for Arctic *Phaeocystis* and *Chaetoceros* (Calbet et al., 2011; Jahnke, 1989; Menden-Deuer et al., 2018). The higher accumulation rates indicate a competitive advantage of *Phaeocystis* over diatoms under the initial experimental conditions contributing to the dominance at the beginning of the experiment. Direct measurements of single cell uptake rates on day 6 yielded comparable C and N uptake rates for *Chaetoceros* and *Phaeocystis* cf. (Fig. 12), but higher uptake rates in *Phaeocystis* compared to diatoms at the onset of the experiment are possible, since we did not measure single cell uptake between days 1 and 5. The single-cell stage of *Phaeocystis*, which was predominantly present in our mesocosm, lacks a nutrient storage mechanism (Veldhuis et al., 1991), opposed to the colonial stage which has been shown to store nitrate and phosphorus in their mucous membrane. Therefore, nutrient uptake and growth are more tightly coupled (Verity et al., 1991), suggesting high growth rates of *Phaeocystis* matching the high nitrate drawdown and resulting in the exponential biomass accumulation of Chl a and POC at the beginning of the experiment (Fig. 3 and 7). A fraction of the nitrate consumed by *Phaeocystis* was likely excreted as DON (Sanderson et al., 2008), resulting in the large unaccounted fraction in the N budget. Meanwhile, nutrient uptake and cell division are inherently decoupled in diatoms due to cell cycle architecture, with silicon uptake relevant to the G2/M phase, while carbon and nitrogen assimilation occur throughout (Martin-Jézéquel et al., 2000). Especially after periods of nutrient limitation diatoms are known to accumulate nutrients, especially nitrate and phosphorus, in their large central vacuole (Collos, 1986; Litchman et al., 2007). This partially explains why *Chaetoceros* uptake rates were comparable to *Phaeocystis* on day 6 yet BSi-based accumulation only became exponential after day 5. Additionally, the BSi pool at experiment onset probably included a detrital fraction from Si-arrested cells, meaning early BSi measurements may underestimate active diatom growth as the diatom pool reproportioned from partly detrital to actively growing (Krause et al., 2010). Both species entered the experiment recovering from nitrate limitation, but *Chaetoceros* faced the additional burden of Si limitation-induced cell cycle arrest in the fjord prior to the experiment. While recovery from Si limitation alone is typically

https://doi.org/10.5194/egusphere-2026-3186
Preprint. Discussion started: 18 June 2026

660 rapid upon resupply (De La Rocha & Passow, 2004), the concurrent N limitation possibly prolonged the overall recovery period in *Chaetoceros* relative to *Phaeocystis*.

The different nutrient storage mechanisms likely also contributed to the bloom succession observed in the mesocosms. The
665 collapse of the initial *Phaeocystis*-dominated bloom and the transition from *Phaeocystis* to *Chaetoceros* coincided with the onset of transient nitrate and phosphate depletion due to the increased consumption by *Phaeocystis* during phase I (Fig. 13).

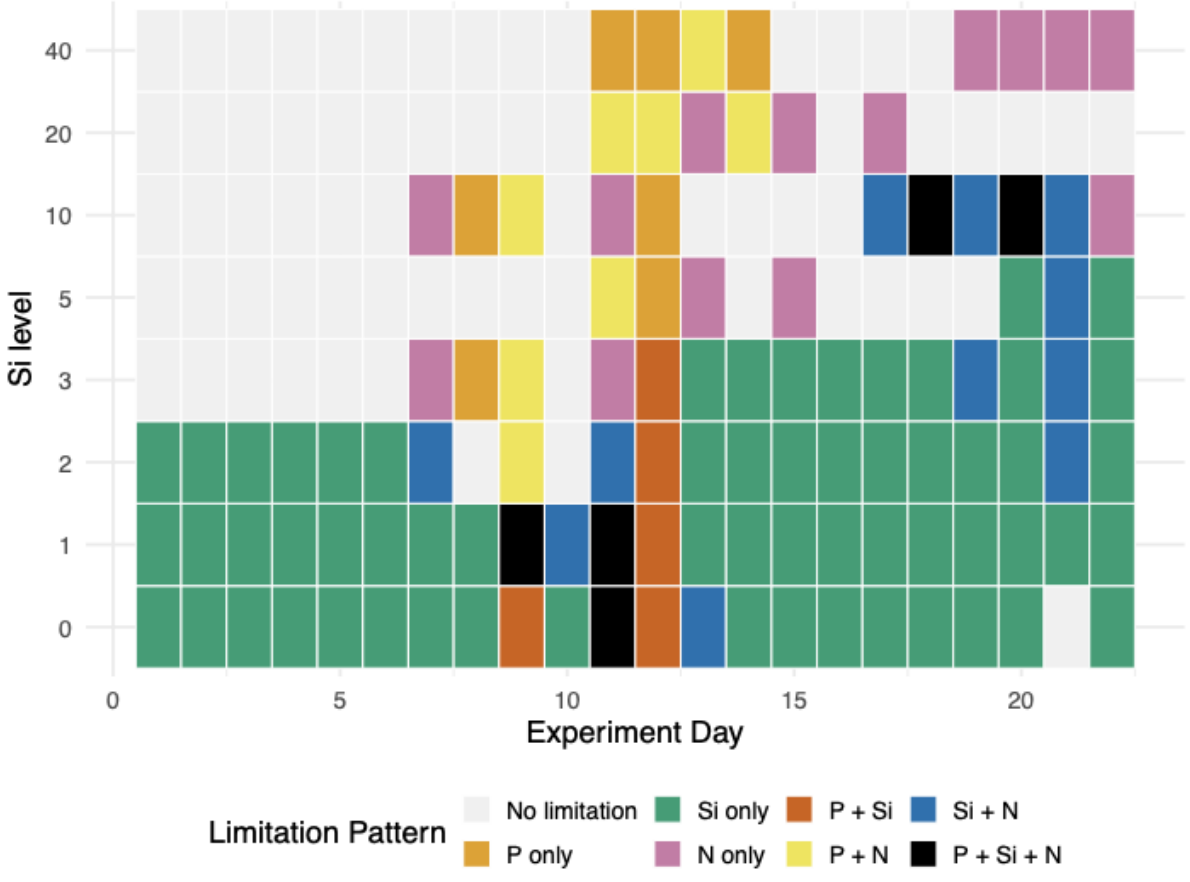

Figure 13: Co-limitation patterns across mesocosms and time. Limitation was defined as 2 µM Si, 0.1 µM phosphate and 1 µM nitrate respectively.

670 In our experiment, Chl *a* based biomass accumulation rates peaked on day 7 followed by a decrease reaching negative growth rates for most mesocosms on day 13 together with single-cell uptake rates for non-diatoms being near zero across mesocosms. The first instance of nitrate drawdown below the threshold of 1 µM commonly considered limiting for phytoplankton (Lewis et al., 2019; Mills et al., 2018) already occurred on day 7 and 8, in select mesocosms. Co-limitation of nitrate and phosphate across the majority of mesocosms occurred on day 11 and 12 supporting the transient nutrient limitation as the main cause of

https://doi.org/10.5194/egusphere-2026-3186
Preprint. Discussion started: 18 June 2026

the *Phaeocystis* bloom collapse. The lack of significant storage abilities of the single cell stage of *Phaeocystis* (Veldhuis et al., 1991) likely provided diatoms with a competitive advantage in dealing with the transient nutrient limitations which resulted from the pulsed nutrient additions during our experiment. In the field, *Chaetoceros* often dominate summer blooms following nutrient inputs into an otherwise limited system (Ardyna et al., 2011; Assmy et al., 2023; Krawczyk et al., 2018). It is important to note that the decline of *Phaeocystis* did not result in a subsequent increase in diatom growth rates. Instead BSi-based diatom accumulation rates reached their maximum already on day 7 supported by the highest *Chaetoceros*-specific nutrient uptake rates measured on day 6 (compare Fig. 4 and 12). Afterwards, BSi accumulation rates continued at a steady level until the end of the experiment (Fig. 3), although *Chaetoceros*-specific nutrient uptake rates continuously decreased. This sustained growth despite transient nutrient limitation is consistent with intracellular nutrient storage allowing *Chaetoceros* to buffer against external limitation (Kamp et al., 2016; Mundy et al., 2025; Twining et al., 2021). The ability to maintain growth rates across a range of nitrogen sources and light regimes has been identified as a key competitive trait of Arctic *Chaetoceros* (Schiffrine et al., 2020) and is consistent with observations of *C. gelidus* dominating subsurface chlorophyll maxima in the post-bloom Beaufort Sea(Martin et al., 2010; Schiffrine et al., 2020), and culture experiments confirm that specific growth rates do not differ significantly between nutrient-rich and nutrient-limited conditions during exponential growth, suggesting a limited physiological penalty under nutrient scarcity (Fierro et al., 2026). Together, the sustained BSi accumulation observed here contrasts with the strong boom-and-bust mechanism commonly associated with diatoms and points instead to a strategy of moderate, persistent growth, which is consistent with the low-nutrient niche occupied by *Chaetoceros*. The continuous decrease of *Chaetoceros* uptake rates after day 6 despite regular macronutrient resupply (Fig. 12) suggests that diatoms experienced increasingly unfavourable growth conditions across the experiment as a result of nitrogen limitation or micronutrient stress. However, the more gradual decline in *Chaetoceros* compared to the rapid collapse of the *Phaeocystis* bloom indicates that diatoms were better able to withstand these conditions, potentially facilitated by their nutrient storage abilities (Kamp et al., 2016; Mundy et al., 2025), allowing for continued biomass accumulation following the bloom transition. In addition to higher nutrient uptake rates by *Phaeocystis* and likely a more direct coupling of uptake rates and growth, other environmental factors could have provided a competitive advantage to *Phaeocystis* over diatoms at the beginning of the experiment. *Phaeocystis* has been reported to correlate negatively with temperature (Calbet et al., 2011; Lasternas and Agustí, 2010). In general, *Phaeocystis* and *Chaetoceros* have been reported to grow under similar temperature ranges in the Arctic, including the range of temperatures present during our study (Hegseth et al., 2019; Simo-Matchim et al., 2017). This suggests that temperature was not a deciding factor for the difference in growth rates between the two species. This is further supported by the drop in temperature around day 17 which did not result in measurable changes in primary productivity or community composition (Fig. 3 and 5). Similarly, light availability is unlikely to have been limiting either species during our experiment. The timing of the experiment in May when the spring bloom was already well underway ensured sufficient light for primary productivity. While we measured some impact of shading by the surrounding harbour structures on our mesocosms the shallow depth of the mesocosms will likely have ensured that the phytoplankton was exposed to similar average light levels as in the fjord with its deeper mixed layer depth. In the field, *Phaeocystis*-dominated communities have demonstrated less efficient

https://doi.org/10.5194/egusphere-2026-3186
Preprint. Discussion started: 18 June 2026

photophysiology and lower primary primary productivity than diatom-dominated communities (Hoppe et al., 2024). The shallow, stratified mesocosm environment may therefore have removed a natural disadvantage of *Phaeocystis* compared to diatoms, which are broadly capable of acclimating to a wide range of light conditions (Lacour et al., 2018; Lomas and Glibert, 1999). This is consistent with higher biomass accumulation rates in *Phaeocystis* reported under well stratified conditions (Assmy et al., 2023). In summary, among bottom-up factors, nutrients were likely the primary determinant of bloom succession, as in the early phase *Phaeocystis* benefited from efficient nitrogen assimilation and tight uptake-growth coupling, while *Chaetoceros* faced the additional burden of recovering from Si limitation-induced cell cycle arrest alongside nitrate limitation in the fjord prior to the experiment. Later, diatoms were more successful at withstanding transient nutrient limitation potentially facilitated by their nutrient storage abilities, while temperature and light played a minor role throughout.

In addition to nutrient-driven bottom-up control, the relative success of *Phaeocystis* and diatoms may also have been influenced by differential top-down mortality, including grazing by microzooplankton. In our experiment we excluded larger grazers by pre-filtering with a 200 µm mesh excluding larger heterotrophic plankton such as copepods or cirripedia larvae which prey on both *Phaeocystis* colonies and diatom chains (Kohlbach et al., 2023; Nejstgaard et al., 2007) from the mesocosms. In terms of smaller heterotrophic plankton, we observed a continuous presence of dinoflagellates based on metabarcoding data throughout the experiment. While metabarcoding likely overestimated their abundance due to the high genome copy-numbers of dinoflagellates (Martin et al., 2022), in microscopy their presence was potentially underestimated due to the high cell densities and the resulting low settling volume potentially undersampling rarer cells. Ciliates were only present at the onset of the experiment and declined rapidly within the first 4 days (Fig. 5 and A3). Heterotrophic dinoflagellates (e.g., *Gyrodinium*, *Protoperidinium*) are key consumers of both *Phaeocystis* as well as large and chain-forming diatoms in the marginal ice zone and Atlantic-influenced waters (Lavrentyev et al., 2019; Sherr and Sherr, 2007, 2009; Stelfox-Widdicombe et al., 2004). They can ingest diatom chains larger than themselves via pallium or engulf feeding (Stelfox-Widdicombe et al., 2004). However, while *Chaetoceros* spp. was predominantly chain forming with the occasional observation of colonies, *Phaeocystis* was mostly present as single cells. Colony formation in *Phaeocystis* is regarded as a grazing avoidance mechanism as the colonial mucus renders the cells less accessible to microzooplankton grazers (Calbet et al., 2011; Ryderheim et al., 2022). Thus its absence may therefore itself indicate low ambient grazing pressure consistent with the observation of high dinoflagellate presence during diatom blooms, suggesting a feeding preference for diatoms over *Phaeocystis* (Seuthe et al., 2011).

Prior to the experiment in the natural fjord environment the spring bloom in 2024 *Chaetoceros* abundances started to increase at the end of March and first *Phaeocystis* colonies started to appear at the end of April with the full bloom composed of *Phaeocystis* and *Chaetoceros* reaching its maximum at the beginning of May coinciding with the start of our experiment (data not shown). The spring bloom in Kongsfjorden often starts with a diatom bloom transitioning from pennate diatoms to centric diatoms, such as *Thalassiosira* (Hegseth et al., 2019). This diatom bloom is mostly succeeded by *Phaeocystis* (Assmy et al., 2023; Hegseth et al., 2019; Hoppe et al., 2024). *Chaetoceros* often occurs later during the bloom, simultaneously to *Phaeocystis*, potentially due to their mutual strategy to avoid predation from small grazers by colony formation. This bloom history and the earlier start of the *Chaetoceros* bloom compared to *Phaeocystis* is likely to affect community succession and

https://doi.org/10.5194/egusphere-2026-3186
Preprint. Discussion started: 18 June 2026

bloom development within our mesocosms for example through pathogen-driven top-down control. Growth rates of *Chaetoceros* as well as *Phaeocystis* are known to be affected by virus or chytrid infections with the ability to control bloom development (Brussaard et al., 2007; Mojica and Brussaard, 2014; Scholz et al., 2017; Tomaru et al., 2008). Infectious control usually gains increasing importance over the course of the bloom (Scholz et al., 2017), which would make *Chaetoceros* more vulnerable to pathogenic control as it occurred in larger abundances in the fjord for a longer period. The Si limitation in the fjord prior to our experiment would have made *Chaetoceros* particularly susceptible to viral infection, supporting viral induced mortality of *Chaetoceros* (Kranzler et al., 2019). Additionally, *Phaeocystis* was predominantly in colonial stage in the fjord prior to our experiment, which is known to be an effective protection against viral infection (Jacobsen et al., 2007). Additionally, the coincidence of *Phaeocystis* collapse with nutrient limitation, indirectly supports that *Phaeocystis* was not controlled by pathogens or viruses, which would have manifested as a bloom collapse independent of nutrient availability (Hoppe et al., 2024). While viral lysis rates or other pathogens were not assessed within the framework of our experiment, this could have provided *Phaeocystis* with a competitive advantage compared to *Chaetoceros* at the onset of our experiment allowing for faster bloom development. Consistent with this, the persistently low but positive growth rates of *Chaetoceros* throughout the experiment may reflect chronic sublethal pathogen pressure compatible with density-dependent infection rather than episodic bloom collapse (Tomaru et al., 2008). Overall, the more rapid accumulation of *Phaeocystis* relative to *Chaetoceros* in the early experimental phase likely reflected a combination of bottom-up and top-down factors. The legacy of Si limitation-induced cell cycle arrest alongside nitrate limitation in the fjord may have initially constrained *Chaetoceros* division, while tighter uptake-growth coupling potentially favoured *Phaeocystis*. Top-down pressure from micrograzers and pathogens may have further contributed, with Si limitation potentially compounding viral infection of *Chaetoceros* (Kranzler et al., 2019).

4.2 Diatom growth dynamics and influence of Si concentration on bloom formation

While the *Phaeocystis* bloom developed independent of Si concentrations, diatom growth showed a strong correlation with Si availability across various parameters (Table 2). Si drawdown rates as well as uptake rates showed a positive linear relationship with Si concentrations. While Si uptake linearly correlated with Si availability across the experiment, in N and P drawdown this correlation was observed only in the second phase of the experiment. This shows that while Si uptake is always diatom-dependent, N and P uptake dynamics were only driven by diatoms during the second bloom, supporting a temporally complex but substantial contribution of diatoms to total primary productivity. Diatom growth follows classic Michaelis-Menten (Monod) saturation kinetics with respect to Si (Nelson et al., 1976). During our experiment, the relationship between Si availability and diatom response was best described by three distinct regimes. Between 0–2 and 0-3 µM Si, multiple biomass proxies (Chl-a, POC, PON) and carbon and nitrate uptake and drawdown rates increased linearly with Si concentration, indicating that growth was Si-limited in this range (Egge and Aksnes, 1992; Krause et al., 2018). No net growth was observed in the Si-free treatment, confirming that sustained biomass accumulation requires a minimum Si supply. Between 5–10 µM Si, drawdown rates, BSi accumulation, and Si uptake rates continued to increase with Si availability, while carbon and nitrate

https://doi.org/10.5194/egusphere-2026-3186
Preprint. Discussion started: 18 June 2026

uptake rates no longer responded, indicating that cells were still kinetically Si-limited with respect to silicification but that this did not translate into growth limitation. This decoupling is consistent with the well-documented capacity of diatoms to maintain division rates under moderate Si stress by reducing frustule silicification, such that the half-saturation constant for growth (Kμ) is considerably lower than that for Si uptake (Ks) (Martin-Jézéquel et al., 2000; McNair et al., 2018). No additional stimulating effects of Si concentrations on nutrient consumption or biomass concentrations were observed beyond 10 μM Si, suggesting that 10 μM Si are sufficient for optimal growth rates, coinciding with the Si concentrations in Kongsfjord after winter mixing (Hegseth et al., 2019). Saturating concentrations for diatoms in field communities around Svalbard are reported between 5-10 μM matching our findings (Krause et al., 2018). These findings underscore the Si-dependent growth of diatoms and highlight that low Si concentrations are not a prerequisite for *Phaeocystis* dominance, but are a limiting factor for diatom competitiveness.

Table 2: Summary of responses to Si availability. Treatment effects across phases and the different pools (dissolved, particulate, exported).

Parameter	Phase I- *Phaeocystis* dominated (Day 0–14)	Phase II-*Chaetoceros* dominated (Day 15–22)
Nutrient Drawdown		
Nitrate drawdown	No effect	**Strong** (ρ=0.59, $p<0.001$; R^2 =0.6 for 0-10 μM)
Phosphate drawdown	No effect	**Moderate** (ρ=0.44, $p<0.01$; R^2= 0.26 for 0-10 μM)
Silicic acid drawdown	No effect	**Very strong** (ρ=0.80, $p<0.001$; R^2 = 0.85 for 0-10 μM)
Bulk Uptake		
Carbon uptake	No effect	**Strong** (ρ=0.76, $p<0.05$)
Nitrogen uptake	No effect	No effect
Silicon uptake	**Very strong** (ρ=0.78, $p<0.001$; R^2=0.68 for 0–10 μM)	**Very strong** (ρ=0.98, $p<0.001$; R^2=0.76 for 0-10 μM)
Single-Cell Uptake (SIMS)		
Chaetoceros C uptake	No effect	**Strong non-monotonic** on day 14: ε^2=0.54, $p<0.001$, optimum at Si 3 μM
Particulate Organic Matter (Water Column)		
POC mean concentration	No effect	**Strong** (ρ=0.74, $p<0.05$)
PON mean concentration	No effect	**Strong** (ρ=0.74, $p<0.05$)
BSi mean concentration	**Very strong** (ρ = 0.9, $p<0.01$)	**Very strong** (ρ = 0.9, $p<0.01$)

https://doi.org/10.5194/egusphere-2026-3186
Preprint. Discussion started: 18 June 2026

Chl *a* mean concentration	**Strong** (ρ=0.7, p<0.05)	No effect
Export Flux		
POC export	515–1102 µmol m^{-2} d^{-1} (Day 7)	**Strong** + (447–2132, max at Si20, Day 22)
PON export	70.9–152 µmol m^{-2} d^{-1} (Day 7)	**Strong** + (64.4–296, Day 22)
BSi export	16.8–41.3 µmol m^{-2} d^{-1} (Day 7)	**Very strong** + (14.4–628, massive at Si20, Day 22)

4.3 Contrasting export dynamics of *Phaeocystis* and *Chaetoceros*

Export dynamics in our experiment were predominantly diatom-mediated, yet overall export efficiency was low. Despite the strong coupling of biogenic silica and carbon export fluxes (Fig. 9), the mass balance analysis and the continued accumulation of POC following the *Phaeocystis* bloom collapse showed that the majority of the biomass was retained in the water column. This matches the extensive literature reporting that *Phaeocystis* in the Arctic is often not exported efficiently (Assmy et al., 2023; Wassmann, 1994) and references therein. After the collapse of the *Phaeocystis* bloom we observed considerable increases in dissolved inorganic phosphate. This is consistent with the release of phosphate stored in the mucous membrane of the colonial stage of *Phaeocystis* (Veldhuis et al., 1991). While the colonial stage was not dominant, small colonies or partial colonies were regularly observed throughout the *Phaeocystis* bloom. The majority of *Phaocystis* biomass was however not fully remineralised based on the high POC concentration and the considerable DON pool suggested by the poor nitrogen budget closure (only 16-34% of added nitrogen were accounted for as inorganic or particulate nitrogen, Fig. 10).

While export fluxes increased markedly by day 22 they nevertheless constituted a minor fraction of the existing biomass (<30% of PON). Several aspects likely contributed to the low export flux even under diatom-dominated conditions. Firstly, the experiment was terminated before the peak of the bloom, hence the collapse of the second bloom which generally dominates export processes during the spring bloom was not resolved by our data (Hufnagel et al., 2026; Lalande et al., 2016). In addition, the dominant diatom *Chaetoceros* is only lightly silicified reducing the ballasting effect and has long setae which results in slow sinking aggregates (Laurenceau-Cornec et al., 2015). Despite the overall low export efficiency, the strong linear relationship between Si addition and N export efficiency (R^2 = 0.75, Table 2), as well as the strong coupling between biogenic silica and particulate organic carbon export fluxes suggests that the fraction of material reaching the sediment trap was either diatom-derived or ballasted by diatoms.

4.4 Implications for the future of Arctic spring bloom dynamics

Our Si gradient mesocosm experiment not only helps to understand the dynamics of different phytoplankton species under controlled conditions, but our findings on nutrient replenishment frequency effects also have direct applicability to understanding phytoplankton community structure in Arctic environments with episodic nutrient injection. However, some experimental limitations need to be considered when extrapolating to Kongsfjorden spring bloom dynamics. The exclusion of

https://doi.org/10.5194/egusphere-2026-3186
Preprint. Discussion started: 18 June 2026

large grazers, particularly calanoid copepods, reduced predation pressure in the mesocosms and likely affected colony formation which can in turn affect nutrient uptake and storage mechanisms (Ploug et al., 1999; Wu et al., 2023). However, overall community dynamics in the mesocosms were in good agreement with phytoplankton succession dynamics in the fjord, where, analogous to the mesocosms the community in May was first dominated by *Phaeocystis* and then shifted to *Chaetoceros* (results not shown), suggesting comparability between mesocosm and fjord dynamics. Additionally, our enclosed mesocosm systems may have experienced micronutrient and transient CO2 limitation that could constrain maximum bloom capacity relative to open fjord conditions. Episodic CO2 limitation during spring blooms has been documented on the West Svalbard shelf even under open ocean conditions, where strong biological drawdown outpaces atmospheric resupply (Sanz-Martín et al., 2018), a constraint likely amplified in our enclosed systems.

Despite these potential biases, our results showed that *Chaetoceros* sustained growth rates despite frequent nutrient limitation in phase II of the experiment, pointing towards a high ability to maintain growth under the stratified, low-nutrient conditions that increasingly characterise the late productive season in Arctic fjord and shelf environments (Fig. 11). This is consistent with the late-bloom niche *Chaetoceros* occupies in Kongsfjorden, where it persists into the post-bloom period under increasing stratification and nutrient depletion (Assmy et al., 2023; Hegseth et al., 2019; Hoppe et al., 2024). The late summer 2019 *Chaetoceros*-dominated bloom in Kongsfjorden was fuelled by silicic acid (>2.7 µM) after the *Phaeocystis*-dominated spring bloom depleted nitrate concentrations (Assmy et al., 2023). This further illustrates how *Chaetoceros* can exploit the stratified, nutrient-depleted post-bloom water column and demonstrates that Si availability can sustain diatom growth when competitive pressure from *Phaeocystis* is reduced. This capacity may become increasingly important under projected Arctic change. Increased water column stratification driven by warming, ice melt, and freshwater input is expected to regionally reduce nutrient fluxes to the euphotic zone (Carmack et al., 2016; McLaughlin and Carmack, 2010). Within the diatom community, such conditions are expected to disadvantage large, nutrient-demanding bloom-formers while favouring taxa capable of sustaining growth under chronic nutrient scarcity (Li et al., 2009; Litchman et al., 2009). Although susceptibility to lytic viral infection is enhanced under stratification-induced Si limitation (Kranzler et al., 2019), *Chaetoceros*, with its ubiquitous presence across Arctic environments and documented capacity for sustained growth under nutrient limitation and high physiological plasticity under variable CO2 and light levels (Biswas, 2022), may be well-positioned to persist under these conditions

Furthermore, our findings support that rather than Si concentrations, differences in nutrient accumulation and growth strategies as well as top-down controls regulate species succession and relatively low Si concentrations (> 1 µM) were sufficient to sustain diatom biomass. This suggests that the reported declining Si concentrations (Hátún et al., 2017; Rey, 2012) might limit the overall magnitude or duration of diatom blooms, but are unlikely to determine bloom dominance. Regardless of Si availability, our findings indicate that under nutrient-replete conditions without transient nutrient limitation, which are increasingly favoured by Atlantification-driven changes in water mass structure (Hegseth and Tverberg, 2013; Lasternas and Agustí, 2010), *Phaeocystis* is likely to expand its dominance due to its ability to achieve high growth rates under sufficient nutrient availabilities. In addition to nutrient availability top-down processes were shown to shape phytoplankton successions.

https://doi.org/10.5194/egusphere-2026-3186
Preprint. Discussion started: 18 June 2026

Microzooplankton grazing has been projected to increase in warmer, more Atlantic-influenced water (Franzè and Lavrentyev, 2017; Lara et al., 2013; Olli et al., 2007). The future prevalence of pathogens and viruses in the Arctic and their role in shaping phytoplankton bloom phenologies are yet poorly understood. In individual cases i.e. viral lysis of *Micromonas polaris* and the presence of diatom-infesting chytrids has been projected to increase under warmer temperatures and sea-ice loss (Kilias et al., 2020; Piedade et al., 2018) supporting their relevance in controlling future phytoplankton bloom dynamics. Ultimately, the trajectory of Arctic phytoplankton communities will be determined not by any single driver, but by the convergence of nutrient regime shifts, altered grazing pressure, and changing pathogen dynamics. These processes collectively favour colonial, grazing-resistant taxa like *Phaeocystis* and nutrient-limitation-tolerant opportunists like *Chaetoceros*, with the option for reduced carbon export efficiency and altered food web structure (Assmy et al., 2023; Hoppe et al., 2024).

4.5 Conclusion

Our mesocosm experiment revealed that ambient Si availability during the experiment itself did not determine initial succession. *Phaeocystis* bloomed rapidly across all Si treatments, while Si limitation prior to the experiment, alongside concurrent nitrate limitation, initally constrained *Chaetoceros* recovery and possibly contributed to the early competitive advantage of *Phaeocystis*. Si concentrations controlled the magnitude of subsequent diatom biomass accumulation, with growth limitation occurring below approximately 2–3 µM Si, and silicification remaining kinetically Si-limited up to 10 µM without corresponding increases in biomass. The transition from *Phaeocystis* to diatom dominance around day 14 coincided with the onset of nitrate and phosphate depletion and was mediated by differences in nutrient storage capacity: *Chaetocoeros* sustained growth rates despite declining ambient nutrient concentrations and decreasing single-cell uptake rates, while *Phaeocystis* single cells—lacking significant storage abilities—exhibited near-zero uptake rates during nutrient limitation. This storage-dependent competitive advantage enabled *Chaetoceros* to sustain transient nutrient limitation and points to its broader capacity to persist under the stratified, low-nutrient conditions increasingly characteristic of the late productive season. Micrograzing pressure further shaped community dynamics, while prior Si limitation may have compounded viral susceptibility in *Chaetoceros*. Vertical export was predominantly diatom-mediated, with biogenic silica and particulate organic carbon fluxes scaling linearly with Si availability, while the Phaeocystis biomass predominantly remained within the water column. Together, these findings point to diverging ecological trajectories under ongoing Arctic change. Under nutrient-replete, Atlantic-influenced conditions *Phaeocystis* is poised to expand its dominance, while stratified, post-bloom environments will increasingly select for nutrient-limitation-tolerant diatoms. The future role of microzooplankton grazing as well as viral and pathogen control in modulating these trajectories remains poorly constrained. These shifts in community composition carries cascading consequences for carbon export efficiency, food web structure, and Si cycling in Arctic pelagic ecosystems.

https://doi.org/10.5194/egusphere-2026-3186
Preprint. Discussion started: 18 June 2026

Appendix A

A1: Comparison of measured and intended dSi concentrations

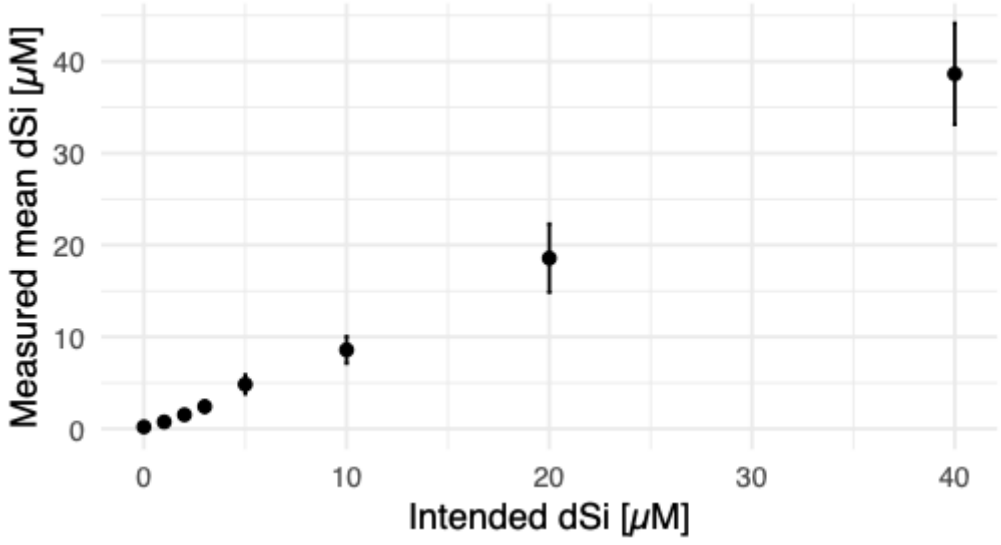

Figure A1: Comparison of measured and intended dSi concentrations. Samples were taken immediately after nutrient addition on every second day of the experiment.

A2: Methods and assay performance of quantitative PCR analysis

Dye-based quantitative PCR (qPCR) assays were performed to evaluate amplification performance for *Phaeocystis pouchetii*. A five-point 10-fold dilution series was prepared in molecular-grade water (Sigma-Aldrich, Steinheim, Germany), ranging from 5 to 5×10^{-4} ng/µL. As no synthetic standards or reference cultures were available, environmental DNA extracts were used as templates for the dilution series. Specifically, sample A30 was used for *Phaeocystis pouchetii*, based on the strong and consistent amplification signals in preliminary assays (S2 A). Standard curves were constructed in triplicate, and the coefficient of determination (R^2), amplification efficiency (E%), and slope were inspected to evaluate assay performance (S2 C). This qPCR reaction mixture contained 1× QIAcuity EvaGreen PCR Kit mastermix (QIAGEN), primers at a final concentration of 400 nM, 2 µL of DNA template, and molecular-grade water to a final volume of 20 µL. Reactions were performed on a QuantStudio 5 Real-Time PCR System (Applied Biosystems) using the same cycling conditions as the subsequent dPCR: an initial denaturation step of 2 min at 95 °C, followed by 40 cycles of 15 s at 95 °C, 15 s at 60 °C, and 15 s at 72 °C. A melting curve analysis was subsequently performed to verify amplification specificity, consisting of 15 s at 95 °C, 30 s at 60 °C, followed by a continuous temperature increase to 95 °C with fluorescence acquisition (S2 B). No Template Controls (NTCs) containing molecular-grade water (Sigma-Aldrich, Steinheim, Germany) instead of DNA template were included in each run as negative control to monitor potential contamination or primer dimers.

https://doi.org/10.5194/egusphere-2026-3186
Preprint. Discussion started: 18 June 2026

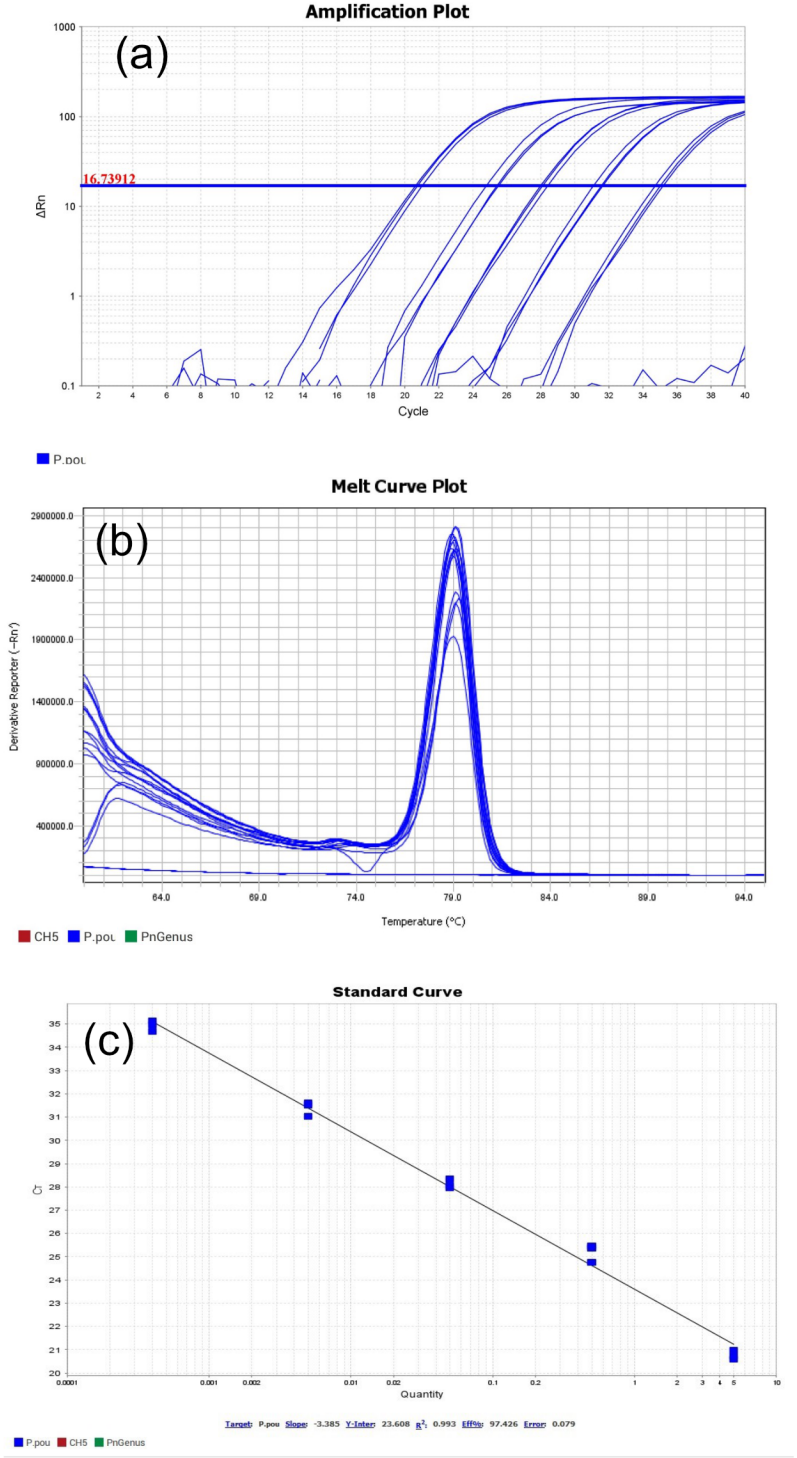

Figure A2: Quality control plots of qPCR for *Phaeocystis*. Amplification plot of 5-point 10 fold dilution series using sample 30 (A). Melt curve plots of T_m dilution series (B) and standard curve of 5-point 10 fold dilution series (C).

https://doi.org/10.5194/egusphere-2026-3186
Preprint. Discussion started: 18 June 2026

A3: Community composition based on 18S amplicon sequencing

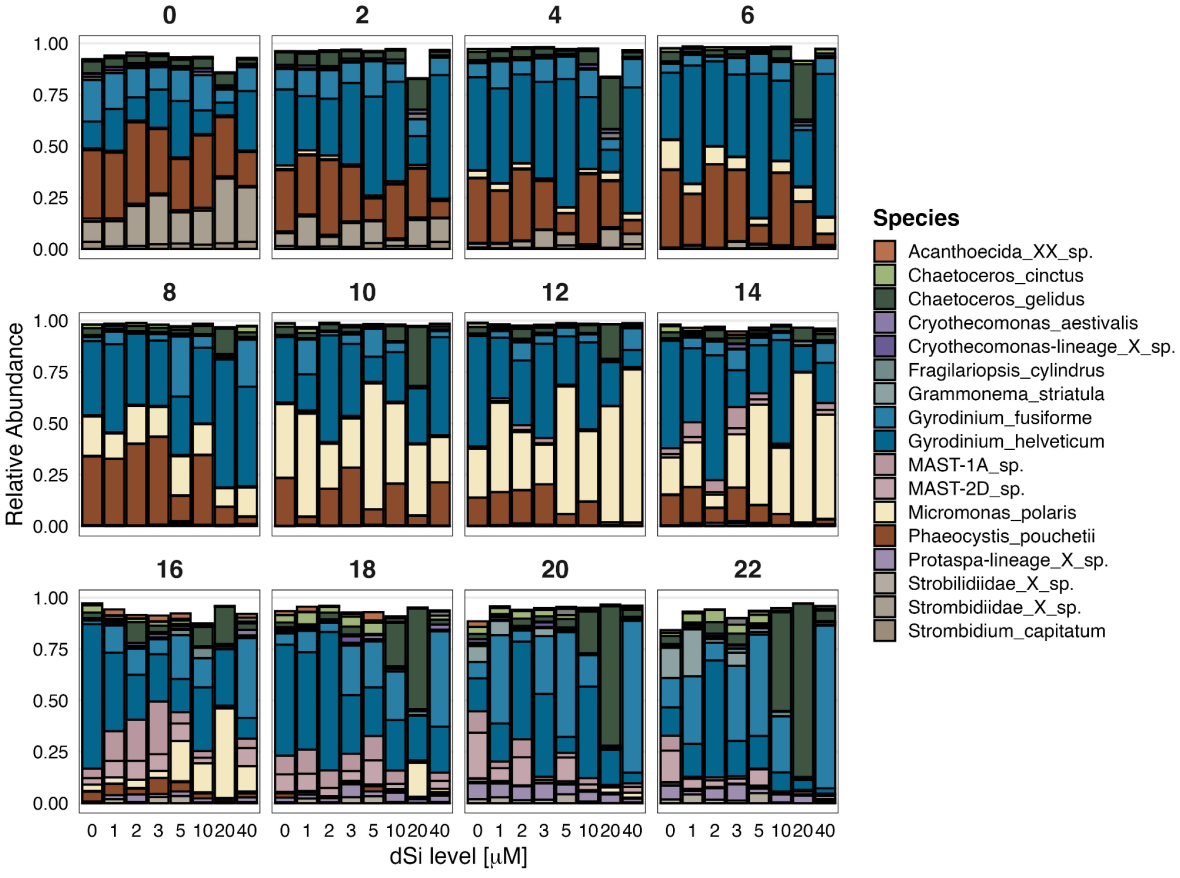

Figure A3: Relative abundance of the most abundant taxa based on 18S sequencing analysis across the Si treatment over time.

https://doi.org/10.5194/egusphere-2026-3186
Preprint. Discussion started: 18 June 2026

A4: *Phaeocystis* abundance

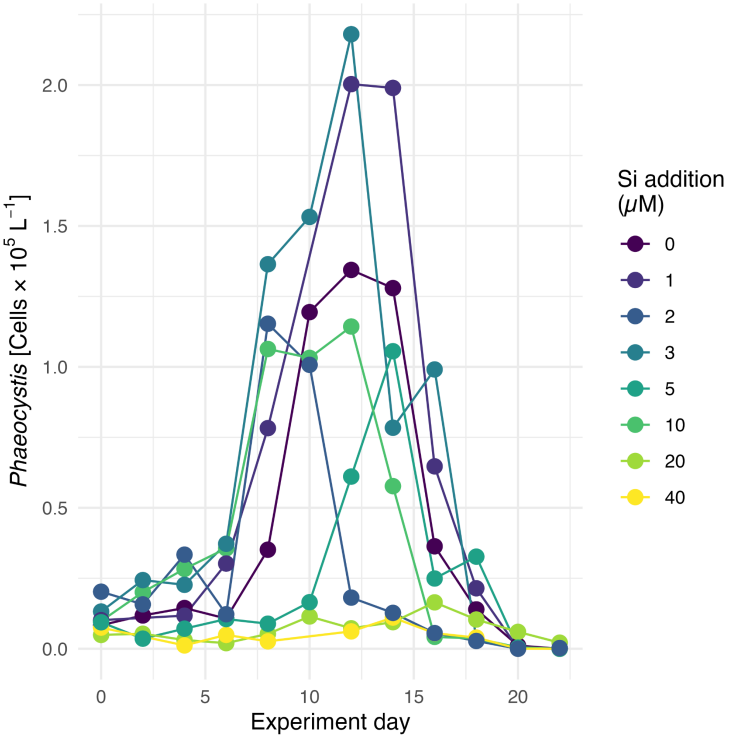

Figure A4: Quantification of Phaeocystis abundance over time via dPCR. 18S genome copy numbers were transformed to cells based on copy number available for Phaeocystis globosa (n = 9) (Chen et al., 2024)

Data availability

All environmental, biogeochemical, and biological data associated with this study have been deposited in the PANGAEA data repository (DOIs are not yet available, but will be added here during the review process). Raw reads from 18S rRNA amplicon sequencing have been deposited in the European Nucleotide Archive (ENA) under accession number PRJEB113818.

Author contributions

AUT and MFM planned the experiment, AUT, MFM, SLE and CH collected data and performed the experiments, AUT, SLE, JWK, UJ, DC, MW, HJ, NC, FC and AC analysed samples and provided data, AUT analysed the data and wrote the manuscript with input from MFM and CJM, all authors reviewed the manuscript

https://doi.org/10.5194/egusphere-2026-3186
Preprint. Discussion started: 18 June 2026

Competing interests

The authors declare that there are no conflicts of interest.

Acknowledgements

We thank the AWIPEV team and Kingsbay for logistical support on site, and Lorenz Eckhard and Kim Vane for their assistance during the field work. We thank Jacqueline Stefels for enabling ^{13}C-DIC measurements and fruitful discussions on the calculation of uptake rates. We are grateful to Elizabeth Robertson for ^{13}C-POC/^{15}N-PON analyses, Mohammad Shahin for help with ^{13}C-DIC, POP and POC/N measurement, Malene Gaasvig-Duus for her help with microscopy analysis, and Kerstin Nachtigall for HPLC analysis. We also thank Sebastian Rokitta for his work in designing the mesocosms.

Funding

This study was supported by the Alfred Wegener Institute Helmholtz Centre for polar and marine research and the Helmholtz Young Investigator Group SiDE-Effect (VH-NG-1600) awarded by Helmholtz to Dr. Mar Fernández-Méndez in 2021. The experimental work was supported by AWI land-based expedition grant AWIPEV_027 and AWIPEV_015.

Bibliography

Admiraal, W. and Venekamp, L. A. H.: Significance of tintinnid grazing during blooms of Phaeocystis pouchetii (haptophyceae) in Dutch coastal waters, Neth. J. Sea Res., 20, 61–66, https://doi.org/10.1016/0077-7579(86)90061-X, 1986.

Ahme, A., Von Jackowski, A., McPherson, R. A., Wolf, K. K. E., Hoppmann, M., Neuhaus, S., and John, U.: Winners and Losers of Atlantification: The Degree of Ocean Warming Affects the Structure of Arctic Microbial Communities, Genes, 14, 623, https://doi.org/10.3390/genes14030623, 2023.

Ardyna, M., Gosselin, M., Michel, C., Poulin, M., and Tremblay, J.: Environmental forcing of phytoplankton community structure and function in the Canadian High Arctic: contrasting oligotrophic and eutrophic regions, Mar. Ecol. Prog. Ser., 442, 37–57, https://doi.org/10.3354/meps09378, 2011.

Ardyna, M., Mundy, C. J., Mayot, N., Matthes, L. C., Oziel, L., Horvat, C., Leu, E., Assmy, P., Hill, V., Matrai, P. A., Gale, M., Melnikov, I. A., and Arrigo, K. R.: Under-Ice Phytoplankton Blooms: Shedding Light on the "Invisible" Part of Arctic Primary Production, Front. Mar. Sci., 7, https://doi.org/10.3389/fmars.2020.608032, 2020.

Årthun, M., Eldevik, T., Smedsrud, L. H., Skagseth, Ø., and Ingvaldsen, R. B.: Quantifying the Influence of Atlantic Heat on Barents Sea Ice Variability and Retreat, J. Clim., 25, 4736–4743, https://doi.org/10.1175/JCLI-D-11-00466.1, 2012.

Assmy, P., Fernández-Méndez, M., Duarte, P., Meyer, A., Randelhoff, A., Mundy, C. J., Olsen, L. M., Kauko, H. M., Bailey, A., Chierici, M., Cohen, L., Doulgeris, A. P., Ehn, J. K., Fransson, A., Gerland, S., Hop, H., Hudson, S. R., Hughes, N., Itkin, P., Johnsen, G., King, J. A., Koch, B. P., Koenig, Z., Kwasniewski, S., Laney, S. R., Nicolaus, M., Pavlov, A. K., Polashenski, C. M., Provost, C., Rösel, A., Sandbu, M., Spreen, G., Smedsrud, L. H., Sundfjord, A., Taskjelle, T., Tatarek,

A., Wiktor, J., Wagner, P. M., Wold, A., Steen, H., and Granskog, M. A.: Leads in Arctic pack ice enable early phytoplankton blooms below snow-covered sea ice, Sci. Rep., 7, 40850, https://doi.org/10.1038/srep40850, 2017.

Assmy, P., Cecilie Kvernvik, A., Hop, H., Hoppe, C. J. M., Chierici, M., Divya David, T., Duarte, P., Fransson, A., García, L. M., Patuła, W., Kwaśniewski, S., Maturilli, M., Pavlova, O., Tatarek, A., Wiktor, J. M., Wold, A., Wolf, K. K. E., and Bailey, A.: Plankton dynamics in Kongsfjorden during two years of contrasting environmental conditions, Prog. Oceanogr., 102996, https://doi.org/10.1016/j.pocean.2023.102996, 2023.

Bach, M. G., Gademann, T., Van Leeuwe, M. A., Elzenga, J. T. M., and Stefels, J.: Coupling of dimethylsulfoniopropionate production and carbon fixation in four temperate phytoplankton species excludes active short-term regulation of dimethylsulfoniopropionate synthesis under increased light-stress, Limnol. Oceanogr., 70, 217–231, https://doi.org/10.1002/lno.12745, 2025.

Baer, S. E., Sipler, R. E., Roberts, Q. N., Yager, P. L., Frischer, M. E., and Bronk, D. A.: Seasonal nitrogen uptake and regeneration in the western coastal Arctic, Limnol. Oceanogr., 62, 2463–2479, https://doi.org/10.1002/lno.10580, 2017.

Behrenfeld, M. J., Halsey, K. H., Boss, E., Karp-Boss, L., Milligan, A. J., and Peers, G.: Thoughts on the evolution and ecological niche of diatoms, Ecol. Monogr., 91, e01457, https://doi.org/10.1002/ecm.1457, 2021.

Bhatt, U. S., Walker, D. A., Walsh, J. E., Carmack, E. C., Frey, K. E., Meier, W. N., Moore, S. E., Parmentier, F.-J. W., Post, E., Romanovsky, V. E., and Simpson, W. R.: Implications of Arctic Sea Ice Decline for the Earth System, Annu. Rev. Environ. Resour., 39, 57–89, https://doi.org/10.1146/annurev-environ-122012-094357, 2014.

Biswas, H.: A story of resilience: Arctic diatom Chaetoceros gelidus exhibited high physiological plasticity to changing CO2 and light levels, Front. Plant Sci., 13, 1028544, https://doi.org/10.3389/fpls.2022.1028544, 2022.

Borchers, H. W.: pracma: Practical Numerical Math Functions, 2025.

Boxhammer, T., Taucher, J., Bach, L. T., Achterberg, E. P., Algueró-Muñiz, M., Bellworthy, J., Czerny, J., Esposito, M., Haunost, M., Hellemann, D., Ludwig, A., Yong, J. C., Zark, M., Riebesell, U., and Anderson, L. G.: Enhanced transfer of organic matter to higher trophic levels caused by ocean acidification and its implications for export production: A mass balance approach, PLoS ONE, https://doi.org/10.1371/journal.pone.0197502, 2018.

Bracher, A., Xi, H., von Appen, W.-J., Mehdipour, E., Metfies, K., McPherson, R., Zeising, M., and Nöthig, E.-M.: Resolving the interannual variability of phytoplankton community composition in Fram strait using ship-based high-frequency spectrophotometric measurements from 2015 to 2024, Deep Sea Res. Part II Top. Stud. Oceanogr., 226, 105568, https://doi.org/10.1016/j.dsr2.2025.105568, 2026.

Brussaard, C. P. D., Bratbak, G., Baudoux, A.-C., and Ruardij, P.: Phaeocystis and its interaction with viruses, Biogeochemistry, 83, 201–215, https://doi.org/10.1007/s10533-007-9096-0, 2007.

Brzezinski, M. A.: The Si:C:N ratio of marine diatoms: Interspecific variability and the effect of some environmental variables, J. Phycol., 21, 347–357, https://doi.org/10.1111/j.0022-3646.1985.00347.x, 1985.

Brzezinski, M. A. and Phillips, D. R.: Evaluation of 32Si as a tracer for measuring silica production rates in marine waters, Limnol. Oceanogr., 42, 856–865, https://doi.org/10.4319/lo.1997.42.5.0856, 1997.

Brzezinski, M. A., Nelson, D. M., Franck, V. M., and Sigmon, D. E.: Silicon dynamics within an intense open-ocean diatom bloom in the Pacific sector of the Southern Ocean, Deep Sea Res. Part II Top. Stud. Oceanogr., 48, 3997–4018, https://doi.org/10.1016/S0967-0645(01)00078-9, 2001.

https://doi.org/10.5194/egusphere-2026-3186
Preprint. Discussion started: 18 June 2026

Calbet, A., Saiz, E., Almeda, R., Movilla, J. I., and Alcaraz, M.: Low microzooplankton grazing rates in the Arctic Ocean during a Phaeocystis pouchetii bloom (Summer 2007): fact or artifact of the dilution technique?, J. Plankton Res., 33, 687–701, https://doi.org/10.1093/plankt/fbq142, 2011.

Callahan, B. J., McMurdie, P. J., Rosen, M. J., Han, A. W., Johnson, A. J. A., and Holmes, S. P.: DADA2: High-resolution sample inference from Illumina amplicon data, Nat. Methods, 13, 581–583, https://doi.org/10.1038/nmeth.3869, 2016.

Carmack, E. C., Yamamoto-Kawai, M., Haine, T. W. N., Bacon, S., Bluhm, B. A., Lique, C., Melling, H., Polyakov, I. V., Straneo, F., Timmermans, M.-L., and Williams, W. J.: Freshwater and its role in the Arctic Marine System: Sources, disposition, storage, export, and physical and biogeochemical consequences in the Arctic and global oceans, J. Geophys. Res. Biogeosciences, 121, 675–717, https://doi.org/10.1002/2015JG003140, 2016.

Chatterjee, S., Semmler, T., Screen, J. A., Furevik, T., Selivanova, J., Raj, R. P., Murukesh, N., and Ravichandran, M.: Atmosphere–Ocean–Sea Ice Feedbacks Sustain Recent Barents Sea Ice Loss despite Cooler Atlantic Water Inflow, J. Clim., 37, 6519–6532, https://doi.org/10.1175/JCLI-D-24-0020.1, 2024.

Chen, N., Xu, Q., Zhu, J., Song, H., He, L., Liu, S., Song, X., Yuan, Y., Chen, Y., Cao, X., and Yu, Z.: Chromosome-scale genome assembly reveals insights into the evolution and ecology of the harmful algal bloom species *Phaeocystis globosa* Scherffel, iScience, 27, 110575, https://doi.org/10.1016/j.isci.2024.110575, 2024.

Cottier, F., Tverberg, V., Inall, M., Svendsen, H., Nilsen, F., and Griffiths, C.: Water mass modification in an Arctic fjord through cross-shelf exchange: The seasonal hydrography of Kongsfjorden, Svalbard, J. Geophys. Res. Oceans, 110, https://doi.org/10.1029/2004JC002757, 2005.

Dąbrowska, A. M., McGovern, M., Mazurkiewicz, M., and Poste, A.: Seasonal patterns and environmental drivers of protistan plankton along a terrestrial–marine gradient in Isfjorden (Svalbard), Front. Mar. Sci., 12, https://doi.org/10.3389/fmars.2025.1631963, 2025.

Degerlund, M. and Eilertsen, H. C.: Main Species Characteristics of Phytoplankton Spring Blooms in NE Atlantic and Arctic Waters (68–80° N), Estuaries Coasts, 33, 242–269, https://doi.org/10.1007/s12237-009-9167-7, 2010.

DeMaster, D. J.: The supply and accumulation of silica in the marine environment, Geochim. Cosmochim. Acta, 45, 1715–1732, https://doi.org/10.1016/0016-7037(81)90006-5, 1981.

Dickson, A. G.: Thermodynamics of the dissociation of boric acid in synthetic seawater from 273.15 to 318.15 K, Deep Sea Res. Part Oceanogr. Res. Pap., 37, 755–766, https://doi.org/10.1016/0198-0149(90)90004-F, 1990.

Downes, P. P., Goult, S. J., Woodward, E. M. S., Widdicombe, C. E., Tait, K., and Dixon, J. L.: Phosphorus dynamics in the Barents Sea, Limnol. Oceanogr., 66, S326–S342, https://doi.org/10.1002/lno.11602, 2021.

Egge, J. and Aksnes, D.: Silicate as regulating nutrient in phytoplankton competition, Mar. Ecol. Prog. Ser., 83, 281–289, https://doi.org/10.3354/meps083281, 1992.

Elskens, M., de Brauwere, A., Beucher, C., Corvaisier, R., Savoye, N., Tréguer, P., and Baeyens, W.: Statistical process control in assessing production and dissolution rates of biogenic silica in marine environments, Mar. Chem., 106, 272–286, https://doi.org/10.1016/j.marchem.2007.01.008, 2007.

Fernández-Méndez, M., Katlein, C., Rabe, B., Nicolaus, M., Peeken, I., Bakker, K., Flores, H., and Boetius, A.: Photosynthetic production in the central arctic ocean during the record sea-ice minimum in 2012, Biogeosciences, 12, 3525–3549, https://doi.org/10.5194/bg-12-3525-2015, 2015.

https://doi.org/10.5194/egusphere-2026-3186
Preprint. Discussion started: 18 June 2026

Fierro, S., Cruz-Flores, R., and Sánchez-Saavedra, M. del P.: Photosynthetic and morphological responses of Chaetoceros sp. to nutrient limitation over culture age, J. Appl. Phycol., 38, 1065–1076, https://doi.org/10.1007/s10811-025-03765-w, 2026.

Franzè, G. and Lavrentyev, P. J.: Microbial food web structure and dynamics across a natural temperature gradient in a productive polar shelf system, Mar. Ecol. Prog. Ser., 569, 89–102, https://doi.org/10.3354/meps12072, 2017.

Fripiat, F., Corvaisier, R., Navez, J., Elskens, M., Schoemann, V., Leblanc, K., André, L., and Cardinal, D.: Measuring production—dissolution rates of marine biogenic silica by ^{30} Si-isotope dilution using a high-resolution sector field inductively coupled plasma mass spectrometer, Limnol. Oceanogr. Methods, 7, 470–478, https://doi.org/10.4319/lom.2009.7.470, 2009.

Gattuso, J.-P., Orr, J., Epitalon, J.-M., and Lavigne, H.: seacarb: Seawater Carbonate Chemistry, , 3.3.4, https://doi.org/10.32614/CRAN.package.seacarb, 2026.

Gilbert, P. M., Lipschultz, F., McCarthy, J. J., and Altabet, M. A.: Isotope dilution models of uptake and remineralization of ammonium by marine plankton, Limnol. Oceanogr., 27, 639–650, https://doi.org/10.4319/lo.1982.27.4.0639, 1982.

Glibert, P. M.: Margalef revisited: A new phytoplankton mandala incorporating twelve dimensions, including nutritional physiology, Harmful Algae, 55, 25–30, https://doi.org/10.1016/j.hal.2016.01.008, 2016.

González-Miguéns, R., Gàlvez-Morante, À., Skamnelou, M., Antó, M., Casacuberta, E., Richter, D. J., Lara, E., Vaulot, D., Del Campo, J., and Ruiz-Trillo, I.: A novel taxonomic database for eukaryotic mitochondrial cytochrome oxidase subunit I gene (eKOI), with a focus on protists diversity, Database J. Biol. Databases Curation, 2025, baaf057, https://doi.org/10.1093/database/baaf057, 2025.

Guillard, R. R. L. and Ryther, J. H.: Studies of marine planktonic diatoms: i. cyclotella nana hustedt, and detonula confervacea (cleve) gran., Can. J. Microbiol., 8, 229–239, https://doi.org/10.1139/m62-029, 1962.

Halbach, L., Kitzinger, K., Hansen, M., Littmann, S., and Benning, L. G.: Single-cell imaging reveals efficient nutrient uptake and growth of microalgae darkening the Greenland Ice Sheet, Nat. Commun., 16, https://doi.org/https://doi.org/10.1038/s41467-025-56664-6, 2025.

Hall, P. 0. J. and Aller, R. C.: Rapid, small-volume, flow injection analysis for SCO2, and NH4+ in marine and freshwaters, Limnol. Oceanogr., 37, 1113–1119, https://doi.org/10.4319/lo.1992.37.5.1113, 1992.

Hansen, H. P. and Koroleff, F.: Determination of nutrients, in: Methods of Seawater Analysis, John Wiley & Sons, Ltd, 159–228, https://doi.org/10.1002/9783527613984.ch10, 1999.

Hátún, H., Azetsu-Scott, K., Somavilla, R., Rey, F., Johnson, C., Mathis, M., Mikolajewicz, U., Coupel, P., Tremblay, J.-É., Hartman, S., Pacariz, S. V., Salter, I., and Ólafsson, J.: The subpolar gyre regulates silicate concentrations in the North Atlantic, Sci. Rep., 7, 14576, https://doi.org/10.1038/s41598-017-14837-4, 2017.

Hegseth, E. N. and Tverberg, V.: Effect of Atlantic water inflow on timing of the phytoplankton spring bloom in a high Arctic fjord (Kongsfjorden, Svalbard), J. Mar. Syst., 113–114, 94–105, https://doi.org/10.1016/j.jmarsys.2013.01.003, 2013.

Hegseth, E. N., Assmy, P., Wiktor, J. M., Wiktor, J., Kristiansen, S., Leu, E., Tverberg, V., Gabrielsen, T. M., Skogseth, R., and Cottier, F.: Phytoplankton Seasonal Dynamics in Kongsfjorden, Svalbard and the Adjacent Shelf, in: The Ecosystem of Kongsfjorden, Svalbard, edited by: Hop, H. and Wiencke, C., Springer International Publishing, Cham, 173–227, https://doi.org/10.1007/978-3-319-46425-1_6, 2019.

https://doi.org/10.5194/egusphere-2026-3186
Preprint. Discussion started: 18 June 2026

Hodal, H., Falk-Petersen, S., Hop, H., Kristiansen, S., and Reigstad, M.: Spring bloom dynamics in Kongsfjorden, Svalbard: nutrients, phytoplankton, protozoans and primary production, Polar Biol., 35, 191–203, https://doi.org/10.1007/s00300-011-1053-7, 2012.

Hop, H., Falk-Petersen, S., Svendsen, H., Kwasniewski, S., Pavlov, V., Pavlova, O., and Søreide, J. E.: Physical and biological characteristics of the pelagic system across Fram Strait to Kongsfjorden, Prog. Oceanogr., 71, 182–231, https://doi.org/10.1016/j.pocean.2006.09.007, 2006.

Hoppe, C. J. M., Wolf, K. K. E., Cottier, F., Leu, E., Maturilli, M., and Rost, B.: The effects of biomass depth distribution on phytoplankton spring bloom dynamics and composition in an Arctic fjord, Elem. Sci. Anthr., 12, 00137, https://doi.org/10.1525/elementa.2023.00137, 2024.

Hoppenrath, M., Elbrächter, M., and Drebes, G.: Marine Phytoplankton, Schweizerbart, 2009.

Hufnagel, L., Ramondenc, S., Konrad, C., von Appen, W.-J., Hofmann, Z., Torres Valdés, S., Stefels, J., Moradi, N., Bracher, A., and Iversen, M. H.: Carbon export in an Arctic frontal system in Fram Strait, Deep Sea Res. Part II Top. Stud. Oceanogr., 105631, https://doi.org/10.1016/j.dsr2.2026.105631, 2026.

Humpert, M.: Bathymetric Arctic Map, The Arctic Institute, 2016.

Husson, B., Bluhm, B. A., Cyr, F., Danielson, S. L., Eriksen, E., Fossheim, M., Geoffroy, M., Hopcroft, R. R., Ingvaldsen, R. B., Jørgensen, L. L., Lovejoy, C., Meire, L., Mueter, F., Primicerio, R., and Winding, M.: Borealization impacts shelf ecosystems across the Arctic, Front. Environ. Sci., 12, https://doi.org/10.3389/fenvs.2024.1481420, 2024.

Jacobsen, A., Larsen, A., Martínez-Martínez, J., Verity, P. G., and Frischer, M. E.: Susceptibility of colonies and colonial cells of Phaeocystis pouchetii (Haptophyta) to viral infection, Aquat. Microb. Ecol., 48, 105–112, https://doi.org/10.3354/ame048105, 2007.

Jahnke, J.: The light and temperature dependence of growth rate and elemental composition of *Phaeocystis globosa* scherffel and *P. Pouchetii* (HAR.) Lagerh. in batch cultures, Neth. J. Sea Res., 23, 15–21, https://doi.org/10.1016/0077-7579(89)90038-0, 1989.

Kamp, A., Stief, P., Bristow, L. A., Thamdrup, B., and Glud, R. N.: Intracellular Nitrate of Marine Diatoms as a Driver of Anaerobic Nitrogen Cycling in Sinking Aggregates, Front. Microbiol., 7, https://doi.org/10.3389/fmicb.2016.01669, 2016.

Kilias, E. S., Junges, L., Šupraha, L., Leonard, G., Metfies, K., and Richards, T. A.: Chytrid fungi distribution and co-occurrence with diatoms correlate with sea ice melt in the Arctic Ocean, Commun. Biol., 3, 183, https://doi.org/10.1038/s42003-020-0891-7, 2020.

Kohlbach, D., Lebreton, B., Guillou, G., Wold, A., Hop, H., Graeve, M., and Assmy, P.: Dependency of Arctic zooplankton on pelagic food sources: New insights from fatty acid and stable isotope analyses, Limnol. Oceanogr., 68, 2346–2358, https://doi.org/10.1002/lno.12423, 2023.

Kraberg, A., Baumann, M., and Dürselen, C.: Coastal Phytoplankton, Dr. Friedrich Pfeil, München, 204 pp., 2010.

Kranzler, C. F., Krause, J. W., Brzezinski, M. A., Edwards, B. R., Biggs, W. P., Maniscalco, M., McCrow, J. P., Van Mooy, B. A. S., Bidle, K. D., Allen, A. E., and Thamatrakoln, K.: Silicon limitation facilitates virus infection and mortality of marine diatoms, Nat. Microbiol., 4, 1790–1797, https://doi.org/10.1038/s41564-019-0502-x, 2019.

https://doi.org/10.5194/egusphere-2026-3186
Preprint. Discussion started: 18 June 2026

Krause, J., Boyette, A., Marquez, I., Pickering, R., and Maiti, K.: Drivers of diatom production and the legacy of eutrophication in two river plume regions of the northern Gulf of Mexico, Front. Mar. Sci., 10, https://doi.org/10.3389/fmars.2023.1162685, 2023.

Krause, J. W., Brzezinski, M. A., Landry, M. R., Baines, S. B., Nelson, D. M., Selph, K. E., Taylor, A. G., and Twiningf, B. S.: The effects of biogenic silica detritus, zooplankton grazing, and diatom size structure on silicon cycling in the euphotic zone of the eastern equatorial Pacific, Limnol. Oceanogr., 55, 2608–2622, https://doi.org/10.4319/lo.2010.55.6.2608, 2010.

Krause, J. W., Duarte, C. M., Marquez, I. A., Assmy, P., Fernández-Méndez, M., Wiedmann, I., Wassmann, P., Kristiansen, S., and Agustí, S.: Biogenic silica production and diatom dynamics in the Svalbard region during spring, Biogeosciences, 15, 6503–6517, https://doi.org/10.5194/bg-15-6503-2018, 2018.

Krause, J. W., Schulz, I. K., Rowe, K. A., Dobbins, W., Winding, M. H. S., Sejr, M. K., Duarte, C. M., and Agustí, S.: Silicic acid limitation drives bloom termination and potential carbon sequestration in an Arctic bloom, Sci. Rep., 9, 8149, https://doi.org/10.1038/s41598-019-44587-4, 2019.

Krawczyk, D. W., Meire, L., Lopes, C., Juul-Pedersen, T., Mortensen, J., Li, C. L., and Krogh, T.: Seasonal succession, distribution, and diversity of planktonic protists in relation to hydrography of the Godthåbsfjord system (SW Greenland), Polar Biol., 41, 2033–2052, https://doi.org/10.1007/s00300-018-2343-0, 2018.

Kuhlisch, C., Althammer, J., Sazhin, A. F., Jakobsen, H. H., Nejstgaard, J. C., and Pohnert, G.: Metabolomics-derived marker metabolites to characterize Phaeocystis pouchetii physiology in natural plankton communities, Sci. Rep., 10, 20444, https://doi.org/10.1038/s41598-020-77169-w, 2020.

Lacour, T., Larivière, J., Ferland, J., Bruyant, F., Lavaud, J., and Babin, M.: The Role of Sustained Photoprotective Non-photochemical Quenching in Low Temperature and High Light Acclimation in the Bloom-Forming Arctic Diatom Thalassiosira gravida, Front. Mar. Sci., 5, https://doi.org/10.3389/fmars.2018.00354, 2018.

Lalande, C., Bauerfeind, E., and Nöthig, E.-M.: Downward particulate organic carbon export at high temporal resolution in the eastern Fram Strait: influence of Atlantic Water on flux composition, Mar. Ecol. Prog. Ser., 440, 127–136, https://doi.org/10.3354/meps09385, 2011.

Lalande, C., Nöthig, E.-M., Bauerfeind, E., Hardge, K., Beszczynska-Möller, A., and Fahl, K.: Lateral supply and downward export of particulate matter from upper waters to the seafloor in the deep eastern Fram Strait, Deep Sea Res. Part Oceanogr. Res. Pap., 114, 78–89, https://doi.org/10.1016/j.dsr.2016.04.014, 2016.

Lara, E., Arrieta, J. M., Garcia-Zarandona, I., Boras, J. A., Duarte, C. M., Agustí, S., Wassmann, P. F., and Vaque, D.: Experimental evaluation of the warming effect on viral, bacterial and protistan communities in two contrasting Arctic systems, Aquat. Microb. Ecol., 70, 17–32, https://doi.org/10.3354/ame01636, 2013.

Lasternas, S. and Agustí, S.: Phytoplankton community structure during the record Arctic ice-melting of summer 2007, Polar Biol., 33, 1709–1717, https://doi.org/10.1007/s00300-010-0877-x, 2010.

Laurenceau-Cornec, E. C., Trull, T. W., Davies, D. M., Rocha, C. L. D. L., and Blain, S.: Phytoplankton morphology controls on marine snow sinking velocity, Mar. Ecol. Prog. Ser., 520, 35–56, https://doi.org/10.3354/meps11116, 2015.

Lavrentyev, P. J., Franzè, G., and Moore, F. B.: Microzooplankton Distribution and Dynamics in the Eastern Fram Strait and the Arctic Ocean in May and August 2014, Front. Mar. Sci., 6, 264, https://doi.org/10.3389/fmars.2019.00264, 2019.

https://doi.org/10.5194/egusphere-2026-3186
Preprint. Discussion started: 18 June 2026

Lewis, K. M., Arntsen, A. E., Coupel, P., Joy-Warren, H., Lowry, K. E., Matsuoka, A., Mills, M. M., van Dijken, G. L., Selz, V., and Arrigo, K. R.: Photoacclimation of Arctic Ocean phytoplankton to shifting light and nutrient limitation, Limnol. Oceanogr., 64, 284–301, https://doi.org/10.1002/lno.11039, 2019.

Li, W. K. W., McLaughlin, F. A., Lovejoy, C., and Carmack, E. C.: Smallest Algae Thrive As the Arctic Ocean Freshens, Science, 326, 539–539, https://doi.org/10.1126/science.1179798, 2009.

Litchman, E., Klausmeier, C. A., and Yoshiyama, K.: Contrasting size evolution in marine and freshwater diatoms, Proc. Natl. Acad. Sci., 106, 2665–2670, https://doi.org/10.1073/pnas.0810891106, 2009.

Liu, Y., Hu, Z., Deng, Y., Shang, L., Gobler, C. J., and Tang, Y. Z.: Dependence of genome size and copy number of rRNA gene on cell volume in dinoflagellates, Harmful Algae, 109, 102108, https://doi.org/10.1016/j.hal.2021.102108, 2021.

Lomas, M. W. and Glibert, P. M.: Temperature regulation of nitrate uptake: A novel hypothesis about nitrate uptake and reduction in cool-water diatoms, Limnol. Oceanogr., 44, 556–572, https://doi.org/10.4319/lo.1999.44.3.0556, 1999.

Lomas, M. W., Baer, S. E., Acton, S., and Krause, J. W.: Pumped Up by the Cold: Elemental Quotas and Stoichiometry of Cold-Water Diatoms, Front. Mar. Sci., 6, https://doi.org/10.3389/fmars.2019.00286, 2019.

Lueker, T. J., Dickson, A. G., and Keeling, C. D.: Ocean *p*CO2 calculated from dissolved inorganic carbon, alkalinity, and equations for *K*1 and *K*2: validation based on laboratory measurements of CO2 in gas and seawater at equilibrium, Mar. Chem., 70, 105–119, https://doi.org/10.1016/S0304-4203(00)00022-0, 2000.

Martin, J., Tremblay, J.-É., Gagnon, J.-M., Tremblay, G., Lapoussière, A., Jose, C., Poulin, M., Gosselin, M., Gratton, Y., and Michel, C.: Prevalence, structure and properties of subsurface chlorophyll maxima in Canadian Arctic waters, Mar. Ecol. Prog. Ser., 412, 69–84, https://doi.org/10.3354/meps08666, 2010.

Martin, J. L., Santi, I., Pitta, P., John, U., and Gypens, N.: Towards quantitative metabarcoding of eukaryotic plankton: an approach to improve 18S rRNA gene copy number bias, Metabarcoding Metagenomics, 6, e85794, https://doi.org/10.3897/mbmg.6.85794, 2022.

Martin-Jézéquel, V., Hildebrand, M., and Brzezinski, M. A.: Silicon Metabolism in Diatoms: Implications for Growth, J. Phycol., 36, 821–840, https://doi.org/10.1046/j.1529-8817.2000.00019.x, 2000.

McLaughlin, F. A. and Carmack, E. C.: Deepening of the nutricline and chlorophyll maximum in the Canada Basin interior, 2003–2009, Geophys. Res. Lett., 37, https://doi.org/10.1029/2010GL045459, 2010.

McNair, H. M., Brzezinski, M. A., and Krause, J. W.: Diatom populations in an upwelling environment decrease silica content to avoid growth limitation, Environ. Microbiol., 20, 4184–4193, https://doi.org/10.1111/1462-2920.14431, 2018.

Menden-Deuer, S. and Lessard, E. J.: Carbon to volume relationships for dinoflagellates, diatoms, and other protist plankton, Limnol. Oceanogr., 45, 569–579, https://doi.org/10.4319/LO.2000.45.3.0569, 2000.

Menden-Deuer, S., Lawrence, C., and Franzè, G.: Herbivorous protist growth and grazing rates at in situ and artificially elevated temperatures during an Arctic phytoplankton spring bloom, PeerJ, 6, e5264, https://doi.org/10.7717/peerj.5264, 2018.

Metfies, K., Schroeder, F., Hessel, J., Wollschläger, J., Micheller, S., Wolf, C., Kilias, E., Sprong, P., Neuhaus, S., Frickenhaus, S., and Petersen, W.: High-resolution monitoring of marine protists based on an observation strategy

https://doi.org/10.5194/egusphere-2026-3186
Preprint. Discussion started: 18 June 2026

integrating automated on-board filtration and molecular analyses, Ocean Sci., 12, 1237–1247, https://doi.org/10.5194/os-12-1237-2016, 2016.

Mikkelsen, D. M., Rysgaard, S., and Glud, R. N.: Microalgal composition and primary production in Arctic sea ice: a seasonal study from Kobbefjord (Kangerluarsunnguaq), West Greenland, Mar. Ecol. Prog. Ser., 368, 65–74, https://doi.org/10.3354/meps07627, 2008.

Mills, M. M., Brown, Z. W., Laney, S. R., Ortega-Retuerta, E., Lowry, K. E., van Dijken, G. L., and Arrigo, K. R.: Nitrogen Limitation of the Summer Phytoplankton and Heterotrophic Prokaryote Communities in the Chukchi Sea, Front. Mar. Sci., 5, https://doi.org/10.3389/fmars.2018.00362, 2018.

Mojica, K. D. A. and Brussaard, C. P. D.: Factors affecting virus dynamics and microbial host–virus interactions in marine environments, FEMS Microbiol. Ecol., 89, 495–515, https://doi.org/10.1111/1574-6941.12343, 2014.

Mundy, C. J., Leu, E., Campbell, K., Galindo, V., Levasseur, M., Poulin, M., Tremblay, J.-É., and Gosselin, M.: Intracellular nutrient storage during ice algal spring blooms in the Canadian high Arctic, iScience, 28, 113148, https://doi.org/10.1016/j.isci.2025.113148, 2025.

Nejstgaard, J. C., Tang, K. W., Steinke, M., Dutz, J., Koski, M., Antajan, E., and Long, J. D.: Zooplankton grazing on Phaeocystis: a quantitative review and future challenges, Biogeochemistry, 83, 147–172, https://doi.org/10.1007/s10533-007-9098-y, 2007.

Nelson, D. M., Goering, J. J., Kilham, S. S., and Guillard, R. R. L.: Kinetics of Silicic Acid Uptake and Rates of Silica Dissolution in the Marine Diatom Thalassiosira Pseudonana, J. Phycol., 12, 246–252, https://doi.org/10.1111/j.1529-8817.1976.tb00510.x, 1976.

Norwegian Polar Institute: Svalbard maps, Norwegian Polar Institute, 2026.

Nöthig, E.-M., Bracher, A., Engel, A., Metfies, K., Niehoff, B., Peeken, I., Bauerfeind, E., Cherkasheva, A., Gäbler-Schwarz, S., Hardge, K., Kilias, E., Kraft, A., Mebrahtom Kidane, Y., Lalande, C., Piontek, J., Thomisch, K., and Wurst, M.: Summertime plankton ecology in Fram Strait—a compilation of long- and short-term observations, Polar Res., 34, 23349, https://doi.org/10.3402/polar.v34.23349, 2015.

Olli, K., Wassmann, P., Reigstad, M., Ratkova, T. N., Arashkevich, E., Pasternak, A., Matrai, P. A., Knulst, J., Tranvik, L., Klais, R., and Jacobsen, A.: The fate of production in the central Arctic Ocean – top–down regulation by zooplankton expatriates?, Prog. Oceanogr., 72, 84–113, https://doi.org/10.1016/j.pocean.2006.08.002, 2007.

Olofsson, M., Robertson, E. K., Edler, L., Arneborg, L., Whitehouse, M. J., and Ploug, H.: Nitrate and ammonium fluxes to diatoms and dinoflagellates at a single cell level in mixed field communities in the sea, Sci. Rep., 9, 1424, https://doi.org/10.1038/s41598-018-38059-4, 2019.

Peperzak, L., Colijn, F., Gieskes, W. W. C., and Peeters, J. C. H.: Development of the diatom- *Phaeocystis* spring bloom in the Dutch coastal zone of the North Sea: the silicon depletion versus the daily irradiance threshold hypothesis, J. Plankton Res., 20, 517–537, https://doi.org/10.1093/plankt/20.3.517, 1998.

Perez, F. F. and Fraga, F.: Association constant of fluoride and hydrogen ions in seawater, Mar. Chem., 21, 161–168, https://doi.org/10.1016/0304-4203(87)90036-3, 1987.

https://doi.org/10.5194/egusphere-2026-3186
Preprint. Discussion started: 18 June 2026

Piedade, G. J., Wesdorp, E. M., Montenegro-Borbolla, E., Maat, D. S., and Brussaard, C. P. D.: Influence of Irradiance and Temperature on the Virus MpoV-45T Infecting the Arctic Picophytoplankter Micromonas polaris, Viruses, 10, 676, https://doi.org/10.3390/v10120676, 2018.

Pierrot, D. E., Wallace, D. W. R., and Lewis, E.: MS Excel Program Developed for CO2 System Calculations, , https://doi.org/10.3334/CDIAC/otg.CO2SYS_XLS_CDIAC105a, 2006.

Ploug, H., Stolte, W., and Jørgensen, B. B.: Diffusive boundary layers of the colony-forming plankton alga Phaeocystis sp.— implications for nutrient uptake and cellular growth, Limnol. Oceanogr., 44, 1959–1967, https://doi.org/10.4319/lo.1999.44.8.1959, 1999.

Polyakov, I. V., Pnyushkov, A. V., Alkire, M. B., Ashik, I. M., Baumann, T. M., Carmack, E. C., Goszczko, I., Guthrie, J., Ivanov, V. V., Kanzow, T., Krishfield, R., Kwok, R., Sundfjord, A., Morison, J., Rember, R., and Yulin, A.: Greater role for Atlantic inflows on sea-ice loss in the Eurasian Basin of the Arctic Ocean, Science, 356, 285–291, https://doi.org/10.1126/science.aai8204, 2017.

R Core Team: R: A language and environment for statistical computing., 2025.

Ramondenc, S., Eveillard, D., Metfies, K., Iversen, M. H., Nöthig, E.-M., Piepenburg, D., Hasemann, C., and Soltwedel, T.: Unveiling pelagic-benthic coupling associated with the biological carbon pump in the Fram Strait (Arctic Ocean), Nat. Commun., 16, 840, https://doi.org/10.1038/s41467-024-55221-x, 2025.

Reigstad, M. and Wassmann, P.: Does Phaeocystis spp. contribute significantly to vertical export of organic carbon?, Biogeochemistry, 83, 217–234, https://doi.org/10.1007/s10533-007-9093-3, 2007.

Renaut, S., Devred, E., and Babin, M.: Northward Expansion and Intensification of Phytoplankton Growth During the Early Ice-Free Season in Arctic, Geophys. Res. Lett., 45, https://doi.org/10.1029/2018GL078995, 2018.

Rey, F.: Declining silicate concentrations in the Norwegian and Barents Seas, ICES J. Mar. Sci., 69, 208–212, https://doi.org/10.1093/icesjms/fss007, 2012.

Riebesell, U., Czerny, J., Von Bröckel, K., Boxhammer, T., Büdenbender, J., Deckelnick, M., Fischer, M., Hoffmann, D., Krug, S. A., Lentz, U., Ludwig, A., Muche, R., and Schulz, K. G.: Technical Note: A mobile sea-going mesocosm system - New opportunities for ocean change research, Biogeosciences, https://doi.org/10.5194/bg-10-1835-2013, 2013.

Ryderheim, F., Hansen, P. J., and Kiørboe, T.: Predator Field and Colony Morphology Determine the Defensive Benefit of Colony Formation in Marine Phytoplankton, Front. Mar. Sci., 9, https://doi.org/10.3389/fmars.2022.829419, 2022.

Sanderson, M. P., Bronk, D. A., Nejstgaard, J. C., Verity, P. G., Sazhin, A. F., and Frischer, M. E.: Phytoplankton and bacterial uptake of inorganic and organic nitrogen during an induced bloom of Phaeocystis pouchetii, Aquat. Microb. Ecol., 51, 153–168, https://doi.org/10.3354/ame01178, 2008.

Sanz-Martín, M., Chierici, M., Mesa, E., Carrillo-de-Albornoz, P., Delgado-Huertas, A., Agustí, S., Reigstad, M., Kristiansen, S., Wassmann, P. F. J., and Duarte, C. M.: Episodic Arctic CO2 Limitation in the West Svalbard Shelf, Front. Mar. Sci., 5, https://doi.org/10.3389/fmars.2018.00221, 2018.

Schiffrine, N., Tremblay, J.-É., and Babin, M.: Growth and Elemental Stoichiometry of the Ecologically-Relevant Arctic Diatom Chaetoceros gelidus: A Mix of Polar and Temperate, Front. Mar. Sci., 6, https://doi.org/10.3389/fmars.2019.00790, 2020.

https://doi.org/10.5194/egusphere-2026-3186
Preprint. Discussion started: 18 June 2026

Schoemann, V., Becquevort, S., Stefels, J., Rousseau, V., and Lancelot, C.: Phaeocystis blooms in the global ocean and their controlling mechanisms: a review, J. Sea Res., 53, 43–66, https://doi.org/10.1016/j.seares.2004.01.008, 2005.

Scholz, B., Küpper, F. C., Vyverman, W., Ólafsson, H. G., and Karsten, U.: Chytridiomycosis of Marine Diatoms—The Role of Stress Physiology and Resistance in Parasite-Host Recognition and Accumulation of Defense Molecules, Mar. Drugs, 15, https://doi.org/10.3390/md15020026, 2017.

Seuthe, L., Rokkan Iversen, K., and Narcy, F.: Microbial processes in a high-latitude fjord (Kongsfjorden, Svalbard): II. Ciliates and dinoflagellates, Polar Biol., 34, 751–766, https://doi.org/10.1007/s00300-010-0930-9, 2011.

Sherr, E. B. and Sherr, B. F.: Heterotrophic dinoflagellates: a significant component of microzooplankton biomass and major grazers of diatoms in the sea, Mar. Ecol. Prog. Ser., 352, 187–197, https://doi.org/10.3354/meps07161, 2007.

Sherr, E. B. and Sherr, B. F.: Capacity of herbivorous protists to control initiation and development of mass phytoplankton blooms, Aquat. Microb. Ecol., 57, 253–262, https://doi.org/10.3354/ame01358, 2009.

Simo-Matchim, A.-G., Gosselin, M., Poulin, M., Ardyna, M., and Lessard, S.: Summer and fall distribution of phytoplankton in relation to environmental variables in Labrador fjords, with special emphasis on Phaeocystis pouchetii, Mar. Ecol. Prog. Ser., 572, 19–42, https://doi.org/10.3354/meps12125, 2017.

Stelfox-Widdicombe, C. E., Archer, S. D., Burkill, P. H., and Stefels, J.: Microzooplankton grazing in *Phaeocystis* and diatom-dominated waters in the southern North Sea in spring, J. Sea Res., 51, 37–51, https://doi.org/10.1016/j.seares.2003.04.004, 2004.

Throndsen, J., Hasle, G. R., and Tangen, K.: PHYTOPLANKTON OF NORWEGIAN COASTAL WATERS, Almater Forlag AS, Oslo, 2007.

Tomaru, Y., Shirai, Y., Suzuki, H., Nagumo, T., and Nagasaki, K.: Isolation and characterization of a new single-stranded DNA virus infecting the cosmopolitan marine diatom Chaetoceros debilis, Aquat. Microb. Ecol., 50, 103–112, https://doi.org/10.3354/ame01170, 2008.

Tomas, C. R., Grethe R. Hasle, Erik E. Syvertsen, Karen A. Steidinger, Karl Tangen, John Throndsen, and Berit R. Heimdal: Identifying Marine Phytoplankton, Academic Press, Cambridge, https://doi.org/10.1016/B978-0-12-693018-4.X5000-9, 1997.

Twining, B. S., Antipova, O., Chappell, P. D., Cohen, N. R., Jacquot, J. E., Mann, E. L., Marchetti, A., Ohnemus, D. C., Rauschenberg, S., and Tagliabue, A.: Taxonomic and nutrient controls on phytoplankton iron quotas in the ocean, Limnol. Oceanogr. Lett., 6, 96–106, https://doi.org/10.1002/lol2.10179, 2021.

Van Heukelem, L. and Thomas, C. S.: Computer-assisted high-performance liquid chromatography method development with applications to the isolation and analysis of phytoplankton pigments, J. Chromatogr. A, 910, 31–49, https://doi.org/10.1016/S0378-4347(00)00603-4, 2001.

Veldhuis, M. j. W., Colijn, F., and Admiraal, W.: Phosphate Utilization in Phaeocystis pouchetii (Haptophyceae), Mar. Ecol., 12, 53–62, https://doi.org/10.1111/j.1439-0485.1991.tb00083.x, 1991.

Verity, P. G., Smayda, T. J., and Sakshaug, E.: Photosynthesis, excretion, and growth rates of Phaeocystis colonies and solitary cells, Polar Res., 10, 117–128, https://doi.org/10.3402/polar.v10i1.6732, 1991.

https://doi.org/10.5194/egusphere-2026-3186
Preprint. Discussion started: 18 June 2026

Verity, P. G., Brussaard, C. P., Nejstgaard, J. C., van Leeuwe, M. A., Lancelot, C., and Medlin, L. K.: Current understanding of Phaeocystis ecology and biogeochemistry, and perspectives for future research, Biogeochemistry, 83, 311–330, https://doi.org/10.1007/s10533-007-9090-6, 2007.

Wang, Q., Wekerle, C., Wang, X., Danilov, S., Koldunov, N., Sein, D., Sidorenko, D., von Appen, W.-J., and Jung, T.: Intensification of the Atlantic Water Supply to the Arctic Ocean Through Fram Strait Induced by Arctic Sea Ice Decline, Geophys. Res. Lett., 47, e2019GL086682, https://doi.org/10.1029/2019GL086682, 2020.

Wassmann, P.: Significance of sedimentation for the termination of Phaeocystis blooms, J. Mar. Syst., 5, 81–100, https://doi.org/10.1016/0924-7963(94)90018-3, 1994.

Wassmann, P., Vernet, M., Mitchell, B., and Rey, F.: Mass sedimentation of Phaeocystis pouchetii in the Barents Sea, Mar. Ecol. Prog. Ser., 66, 183–195, https://doi.org/10.3354/meps066183, 1990.

Wassmann, P., Ratkova, T., Andreassen, I., Vernet, M., Pedersen, G., and Rey, F.: Spring Bloom Development in the Marginal Ice Zone and the Central Barents Sea, Mar. Ecol., 20, 321–346, https://doi.org/10.1046/j.1439-0485.1999.2034081.x, 1999.

Weisse, T., Grimm, N., Hickel, W., and Martens, P.: Dynamics of Phaeocystis pouchetii blooms in the Wadden Sea of Sylt (German Bight, North Sea), Estuar. Coast. Shelf Sci., 23, 171–182, https://doi.org/10.1016/0272-7714(86)90052-1, 1986.

Weisse, T., Tande, K., Verity, P., Hansen, F., and Gieskes, W.: The trophic significance of Phaeocystis blooms, J. Mar. Syst., 5, 67–79, https://doi.org/10.1016/0924-7963(94)90017-5, 1994.

Wickham, H.: ggplot2 - Elegant graphics for data analysis, Springer International Publishing, Cham, https://doi.org/10.1007/978-3-319-24277-4, 2016.

Wickham, H., Averick, M., Bryan, J., Chang, W., McGowan, L. D., François, R., Grolemund, G., Hayes, A., Henry, L., Hester, J., Kuhn, M., Pedersen, T. L., Miller, E., Bache, S. M., Müller, K., Ooms, J., Robinson, D., Seidel, D. P., Spinu, V., Takahashi, K., Vaughan, D., Wilke, C., Woo, K., and Yutani, H.: Welcome to the Tidyverse, J. Open Source Softw., 4, 1686, https://doi.org/10.21105/joss.01686, 2019.

Wu, K., Tang, S., Wu, X., Zhu, J., Song, J., Zhong, Y., Zhou, J., and Cai, Z.: Colony formation of *Phaeocystis globosa*: A case study of evolutionary strategy for competitive adaptation, Mar. Pollut. Bull., 186, 114453, https://doi.org/10.1016/j.marpolbul.2022.114453, 2023.